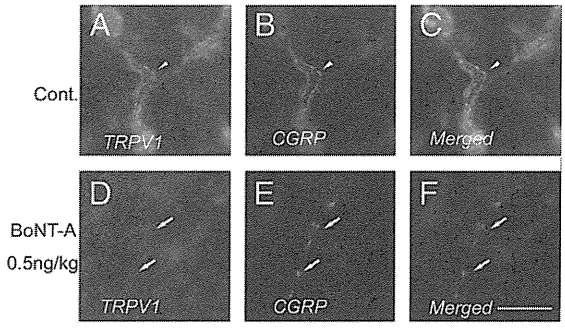

Fig. 3. TRPV1-IR nerve fibers were reduced by BoNT-A treatment of the facial dermis. Double labeling for TRPV1 (green; A, D) and CGRP (red; B, E) in the facial dermis of control (A–C) and 0.5 ng/kg BoNT-A (D–F) groups. (C) Merged image of (A) and (B). (F) Merged image of (D) and (E). As indicated by the arrowheads, the CGRP-IR nerve fibers (B) colocalized with TRPV1-IR (A). As indicated by the arrows, the CGRP-IR nerve fibers (E) did not colocalize with TRPV1-IR (D). Scale bar: 50 μm for all images. (For interpretation of the references to color in this figure legend, the reader is referred to the web version of this article.)

the face skin (82 ± 46 times; n = 11; Fig. 6A open bar). However, animals that received an injection of 0.5 ng/kg BoNT-A into the left side of the face 7 days earlier (Fig. 6A, solid bar) had a significantly lower number of wipes (29 ± 26 times; n = 10) compared to caps (*$p < 0.001$, one-way ANOVA followed by Scheffé's post hoc test). Likewise, animals pretreated with 10 mM capsazepine (Fig. 6A, gray bar) had a significantly decreased number of wipes (26 ± 14 times; n = 9) compared to caps (*$p < 0.001$). There was no significant difference in the number of wipes between the capsazepine-pretreated and BoNT-A-injected animals.

Next, we assessed the selectivity of the BoNT-A action by examining the effect of BoNT-A pretreatment on $P2X_3$-mediated nociception. The injection of a well-established $P2X_3$ agonist, α,β-methyleneATP, to the lateral facial skin did not elicit any nocifensive behaviors. However, the threshold for the induction of nocifensive behavior (head withdrawal and wipes with the forelimb over the skin) with von Frey hair (VFH) stimulation was lowered, which was interpreted as the development of mechanical allodynia. We estimated the number of nocifensive responses to 10 times VFH stimulation before and after injection of

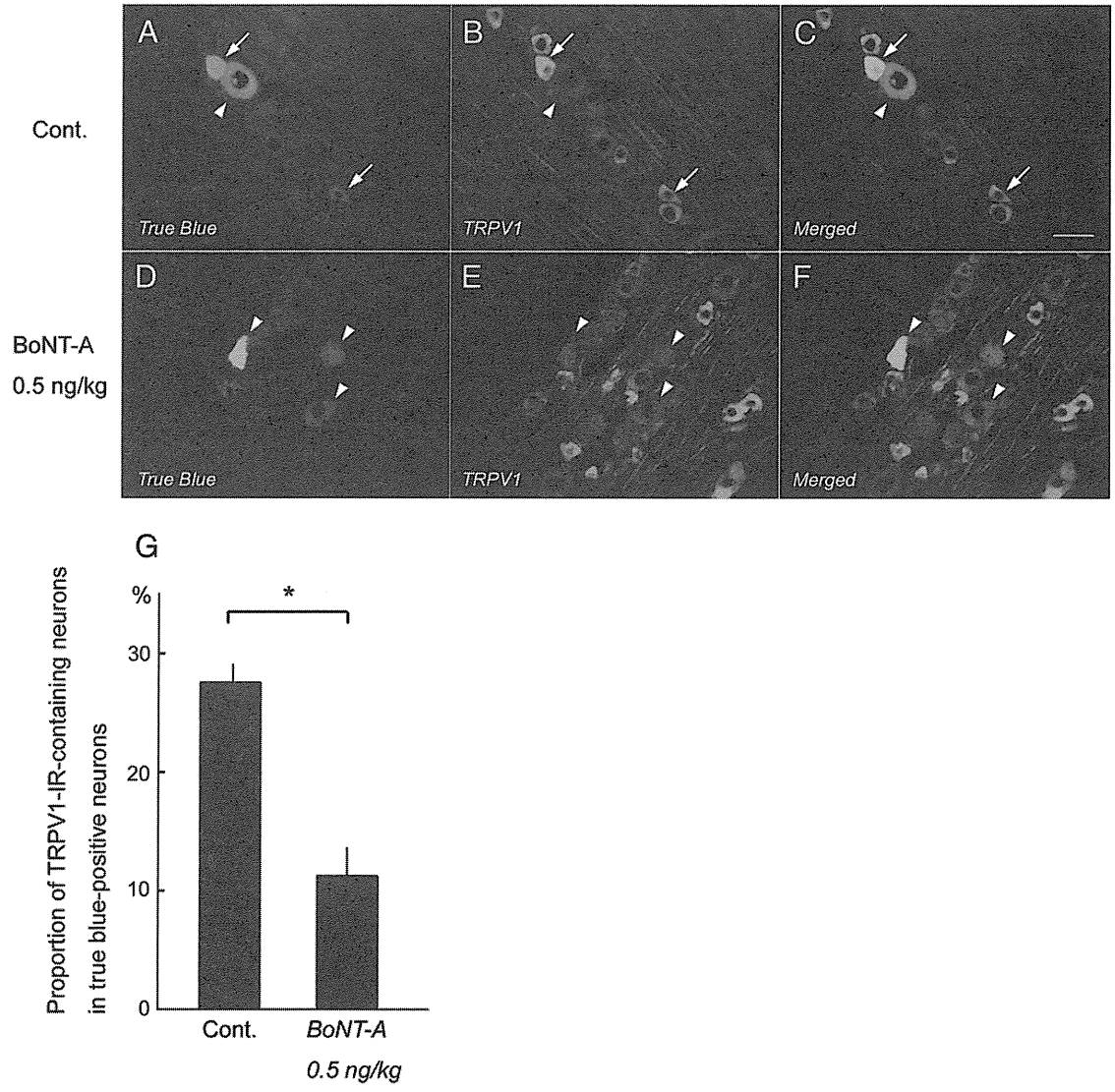

Fig. 4. Reduced number of TRPV1-IR neurons innervating the dura mater after BoNT-A treatment in the TG. Sections of the TG containing neurons retrogradely labeled with true blue (A, D) and TRPV1-IR (B, E). (C) Merged image of (A) and (B). (F) Merged image of (D) and (E). In control (A–C), neurons retrogradely labeled with true blue (A) colocalized with TRPV1-IR (B) are indicated by arrows, and true blue-containing neurons without TRPV1-IR are indicated by arrowheads. In BoNT-A-treated animals (D–F; injected with 0.5 ng/kg BoNT-A containing 1% true blue solution), most of the neurons retrogradely labeled with true blue did not colocalize with TRPV1-IR (arrowheads). Scale bar: 50 μm for all images. (G) Histogram summarizing the quantitative data on the proportion of TRPV1-IR-containing neurons in true blue-positive neurons. Differences between means were considered statistically significant at $p < 0.0001$ (Student's *t*-test).

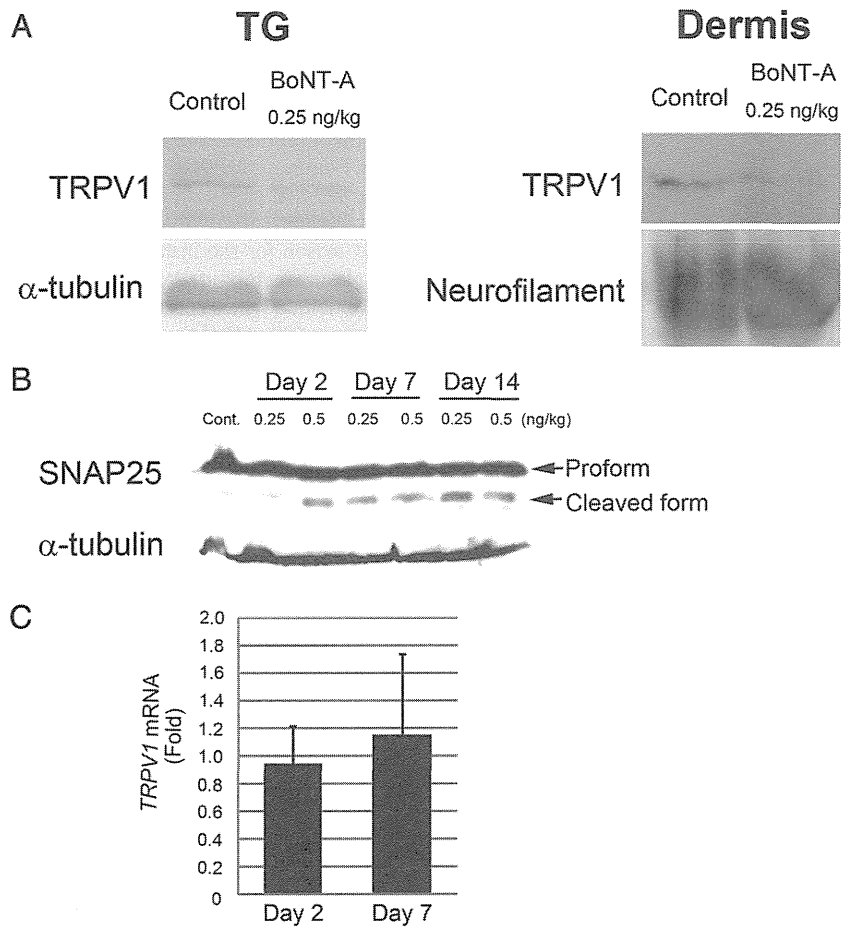

Fig. 5. The BoNT-A-induced reduction in TRPV1 protein expression was not mediated by transcriptional downregulation. (A) BoNT-A administration (0.25 ng/kg) reduced TRPV1 protein expression levels in the TG and facial dermis that contained trigeminal terminals on Day 7. Neurofilament was used to assess the equality of trigeminal nerve-derived protein loading for the dermal samples. (B) Western blot analysis indicated that BoNT-A-mediated cleavage of SNAP25 occurred on Day 2 in a dose-dependent manner. At later time points (Days 7 and 14), SNAP25 cleavage was clearly observed in animals that had received either dose (0.25 or 0.5 ng/kg) of BoNT-A. (C) Quantitative RT-PCR analysis using TaqMan® probes did not reveal significant changes in *TRPV1* transcript levels at Days 2 or 7 after BoNT-A administration (0.5 ng/kg). Statistical significance was set at $p<0.05$ (one-way ANOVA followed by Scheffé's post hoc test).

α,β-methyleneATP into the left lateral face in control animals (Fig. 6B, solid circles; $n=5$) and animals pretreated with 0.5 ng/kg BoNT-A (Fig. 6B, open circles; $n=5$). In control animals, the number of nocifensive responses was 2.0 ± 1.8 times before α,β-methyleneATP injection (before), 4.6 ± 2.3 times at 5 min, 5.4 ± 4.5 times at 20 min and 5.4 ± 4.4 times at 30 min. The number of nocifensive responses after drug administration was significantly increased compared with the baseline value (*$p<0.001$, one-way ANOVA followed by Scheffé's post hoc test). In BoNT-A-pretreated animals, the number of nociceptive response was 1.4 ± 1.5 times before α,β-methyleneATP injection, 6.4 ± 2.1 times at 5 min, 5.4 ± 3.5 times at 20 min and 5.4 ± 3.7 times at 30 min. The number of nocifensive responses was significantly increased after the drug administration compared with the value before α,β-methyleneATP injection (*$p<0.001$, ANOVA followed by Scheffé's post hoc test). However, two-way ANOVA did not detect significant differences in the number of nocifensive responses between the control and BoNT-A-pretreated groups, and BoNT-A pretreatment failed to affect $P2X_3$-mediated threshold alterations.

Next, we performed a surface protein biotin-labeling assay in TG primary neurons. Approximately 90% of TRPV1-positive cells were also CGRP positive (Fig. 7A). In our cultures, BoNT-A was capable of cleaving SNAP25 in a dose-dependent fashion in the range of 0.1–10 nM (Fig. 7B). As BoNT-A has been recognized as a neurotoxin, we first examined the effect of BoNT-A on cell viability. TG neurons did not exhibit any morphological change suggestive of cell death (Fig. 7C) or caspase-3 activation (data not shown) when subjected to 1 nM BoNT-A for 24 h. We treated TG primary cultures with either 1 nM BoNT-A or vehicle for 24 h before labeling cell surface proteins with biotin. We then examined TRPV1 and $P2X_3$ levels in whole cell lysates and eluates from NeutrAvidin agarose beads (biotinylated fractions). We compared the ratios of TRPV1 in the biotinylated fraction to that in the corresponding whole cell lysate and found a reduction to $20.6\pm30.9\%$ in the BoNT-A-treated sample compared to the control (vehicle-treated) sample (Figs. 7D and E). The biotin-labeled $P2X_3$ level was not altered by BoNT-A treatment (Fig. 7E). Such differential actions of BoNT-A were consistent with the behavioral analysis results. To verify the efficiency of biotinylation in each sample, we also looked at biotin-labeled Na/K-ATPase, a representative membrane-bound protein. The results excluded the possibility that the decrease in biotinylated TRPV1 in the BoNT-A-treated fraction was due to inefficient cell surface biotin labeling. We also observed that the BoNT-A treatment caused decreased total TRPV1 expression in TG primary neurons (Fig. 7F).

We then addressed whether impaired trafficking of TRPV1 to the plasma membrane explained the decline in TRPV1 expression. Phosphorylation at tyrosine residue 200 (Y200) is critical for plasma membrane trafficking of TRPV1 (Zhang et al., 2005). We synthesized expression plasmids encoding enhanced GFP (EGFP)-tagged wild-type TRPV1 and mutant TRPV1 (tyrosine 200 to phenylalanine, Y200F), and these plasmid vectors were transfected into PC12 cells. We found that EGFP-tagged Y200F TRPV1 mutant was poorly translocated to the plasma membrane, whereas the EGFP-tagged wild-type TRPV1 was appropriately

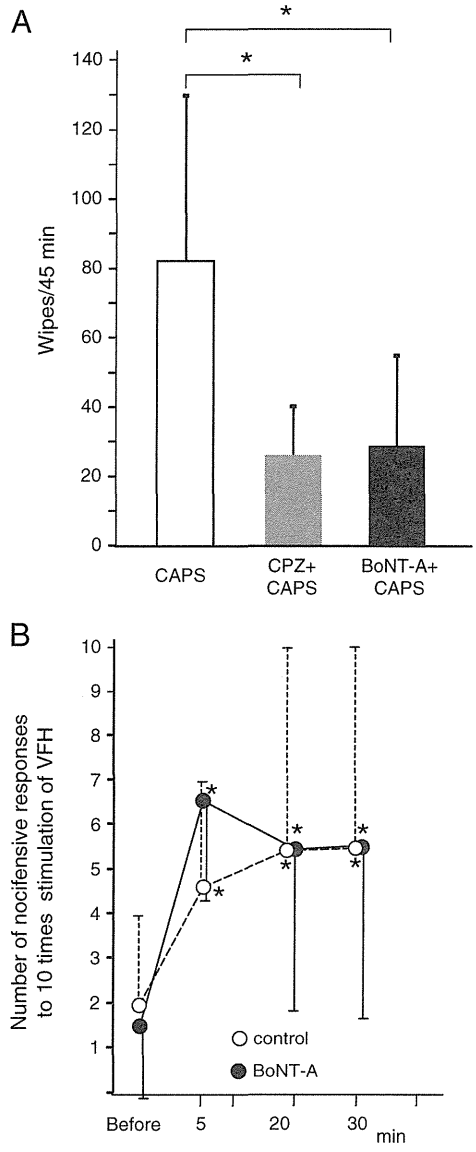

Fig. 6. Effects of BoNT-A on capsaicin-induced nocifensive behaviors. A. The number of wipes of the left face was counted over 45 min after application of a cotton patch soaked with 10 mM capsaicin to the left side of the face for 30 s. B. The number of nocifensive responses to 10 times stimulation using VFH before and after injection of the $P2X_3$ agonist α,β-methyleneATP into the left lateral face in control animals (solid circles) and animals pretreated with 0.5 ng/kg BoNT-A 7 days previously (open circles). In both groups, there was a significant increase of the number of nocifensive responses after drug administration compared with the baseline value (*$p<0.001$, one-way ANOVA followed by Scheffé's post hoc test). Two-way ANOVA did not detect significant differences in the number of nocifensive responses between the control and BoNT-A-pretreated groups.

localized in the plasma membrane (Fig. 8A). Western blot analysis demonstrated that Y200F TRPV1 expression was much lower than that of the wild-type TRPV1 (Fig. 8B). The results implied that impaired plasma membrane trafficking of TRPV1 led to reduced expression levels. However, at this point, a causal link between the two phenomena was unclear. We hypothesized that a certain degradation mechanism might affect cytoplasmic TRPV1. We investigated whether the ubiquitin-proteasome or lysosome-mediated protein degradation system might be involved in cytoplasmic TRPV1 proteolysis. First, we treated PC12 cells expressing either the wild-type or Y200F-mutant TRPV1 with MG-132, a well-established proteasome inhibitor (Goldberg, 2003), for 24 h. This treatment increased the expression levels of both types of TRPV1 in a dose-dependent manner (wild-type: 181.3 ± 37.2% at 1 μM, 291.4 ± 59.3% at 5 μM; Y200F: 271.6 ± 60.4% at 1 μM, 838.7 ± 189.2% at 5 μM), which indicated that proteasomal degradation was implicated in TRPV1 catabolism (Figs. 8C, E). The immunoreactivity in the high molecular range appeared to represent poly-ubiquitinated EGFP–TRPV1 proteins (Fig. 8C). In addition, MG-132-induced potentiation of protein expression was more robust in the cells expressing Y200F-mutant TRPV1 than in cells expressing wild-type TRPV1. This indicated that cytoplasmic TRPV1 was more vulnerable to proteasomal degradation than plasma membrane-bound TRPV1, which provided a good reason for the instability of TRPV1 that failed to translocate to the plasma membrane. We also assessed the effects of lysosomal protease inhibition with a cocktail of E64d (30 μM), pepstatin A (15 μM), and leupeptin (20 μM) (Mizushima et al., 2010). This intervention did not alter wild-type or Y200F-mutant TRPV1 expression levels (wild-type, 104.6 ± 17.6%; Y200F, 104.3 ± 12.5%), indicating that lysosomal proteases did not play a major role in TRPV1 catabolism (Figs. 8D, E).

Discussion

This study demonstrated that subcutaneous BoNT-A administration to the region of the face innervated by the ophthalmic division of the trigeminal nerve causes SNAP25 cleavage in TG neurons and decreases TRPV1 protein expression in both trigeminal terminals and neurons independently of transcriptional downregulation. Notably, TG neurons that exhibited reduced TRPV1 expression after BoNT-A treatment contained those receiving projections from the dura mater. Pain behavior analysis showed that BoNT-A treatment attenuated TRPV1-mediated nocifensive behaviors. The antinociceptive action of BoNT-A appeared selective because it did not affect $P2X_3$-mediated pain-induced behaviors. In our primary TG neuronal cultures, BoNT-A treatment concomitantly induced SNAP25 cleavage and reduced TRPV1 protein expression. More importantly it inhibited TRPV1 trafficking to the plasma membrane, implying that the exocytosis-mediated TRPV1 delivery system is an important therapeutic target of BoNT-A. Moreover, the pharmacological assay using Y200F-mutant TRPV1 revealed that TRPV1 is prone to ubiquitination and subsequent proteasomal degradation, especially when its plasma membrane trafficking is blocked, which accounted for its decreased expression levels following BoNT-A treatment (Fig. 9).

Our Western blot data clearly demonstrated cleaved SNAP25 in the TG after local BoNT-A administration in the vicinity of trigeminal terminals, which implies that BoNT-A effects are not localized; rather, BoNT-A can affect neuronal somata that project axons to injection sites. Antonucci et al. (2008) histologically demonstrated that BoNT-A can be retrogradely transported, and even transcytosed, to afferent synapses (Antonucci et al., 2008). Moreover, Matak et al. (2011) confirmed the appearance of BoNT-A-truncated SNAP-25 in the trigeminal nucleus caudalis (TNC) neurons after BoNT-A administration to the whisker pad, which was abolished by pretreatment with colchicine (Matak et al., 2011). Their observation provided clear evidence for transcytosis of peripherally-administered BoNT-A up to the brainstem. Our observation that TG neurons innervating the dura mater also had decreased TRPV1 expression strongly suggests that the effect of BoNT-A is not restricted to neurons directly treated with the toxin. In this regard, Kitamura et al. (2009) demonstrated that intradermal administration of BoNT-A to the whisker pad induced a potent inhibition of the vesicular neurotransmitter release from the acutely dissociated TG neurons, which was indicative of the occurrence of transcytosis within TG (Kitamura et al., 2009). Taken together, our data lend support to accumulating evidence for active transcytosis of BoNT-A within the sensory nervous system.

A TRPV1-null mouse study confirmed that TRPV1 plays a pivotal role in the development of inflammatory thermal hyperalgesia (Caterina et al., 2000). In addition, it is known that TRPV1 function can be enhanced by increased plasma membrane expression levels and/or upregulation of TRPV1 cation channel activity, and TRPV1 phosphorylation is important in these phenomena (Bhave et al., 2003; Bonnington and McNaughton,

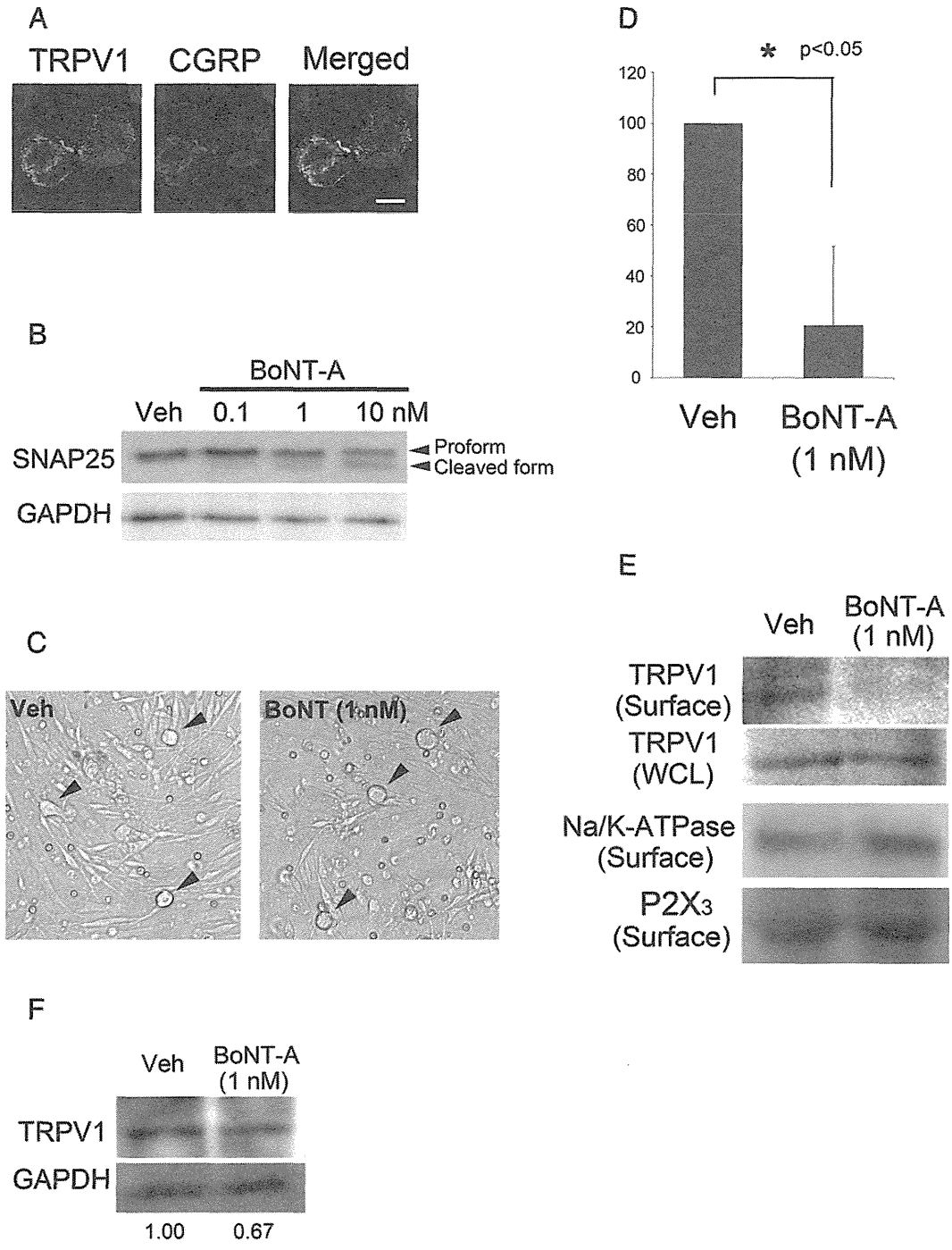

Fig. 7. BoNT-A inhibited TRPV1 trafficking to the plasma membrane in TG neurons. (A) TRPV1 immunostaining showed that TRPV1 was expressed in CGRP-positive small-diameter (~20 μm) neurons. Approximately 90% of TRPV1-positive cells were immunoreactive for CGRP. Green: TRPV1; red: CGRP; blue: nuclei; scale bar: 10 μm. (B) BoNT-A cleaved SNAP25 in a dose-dependent manner in the range of 0.1–10 nM. The molecular weights of the pro and cleaved forms were 25 and 23 kDa, respectively. The blot was probed for GAPDH to confirm equal sample loading. (C) BoNT-A (1 nM) treatment for 24 h did not result in any morphological changes suggestive of cell death. Arrowheads indicate TG neurons. (D) The ratio of TRPV1 in the plasma cell (biotinylated) fraction to that in the whole cell lysate was significantly reduced to 20.6±30.1% ($p<0.05$, Student's *t*-test) in the BoNT-A-treated cell culture compared to the vehicle-treated cell culture. The bar represents SD. (E) Cell surface biotin labeling indicated that TRPV1 plasma membrane expression in TG neurons decreased 24 h after BoNT-A (1 nM) treatment. The decrease in TRPV1 band intensity in the biotinylated fraction sample was obvious, even after the whole cell lysate TRPV1 level in the BoNT-A-treated sample was matched with that in the vehicle-treated sample. BoNT-A treatment did not affect $P2X_3$ cell surface expression. The identical whole cell lysate and biotinylated protein samples were examined for Na/K-ATPase α subunit, a representative plasma membrane protein, which confirmed that the decreased biotinylated TRPV1 level induced by BoNT-A treatment was not due to inefficient biotin labeling. (F) BoNT-A reduced TRPV1 expression in the whole cell lysate of the TG culture. As indicated by the numbers below the blots, quantification revealed that BoNT-A (1 nM) treatment for 24 h reduced TRPV1 level, normalized by the GAPDH level by 33%. The blots were representative of three independent experiments. (For interpretation of the references to color in this figure legend, the reader is referred to the web version of this article.)

2003; Gunthorpe and Chizh, 2009; Morenilla-Palao et al., 2004; Stein et al., 2006; Zhang et al., 2005; Zhu and Oxford, 2007). In particular, Y200 phosphorylation of TRPV1 was found to be crucial in plasma membrane translocation evoked by NGF, an algogenic inflammatory mediator that acts on the tyrosine kinase receptor, TrkA (Zhang et al., 2005). As our PC12 cells were grown in NGF-free medium, the basal trafficking of TRPV1 to the plasma membrane in our cultures was largely dependent on Y200 phosphorylation. NGF-induced Y200 phosphorylation of

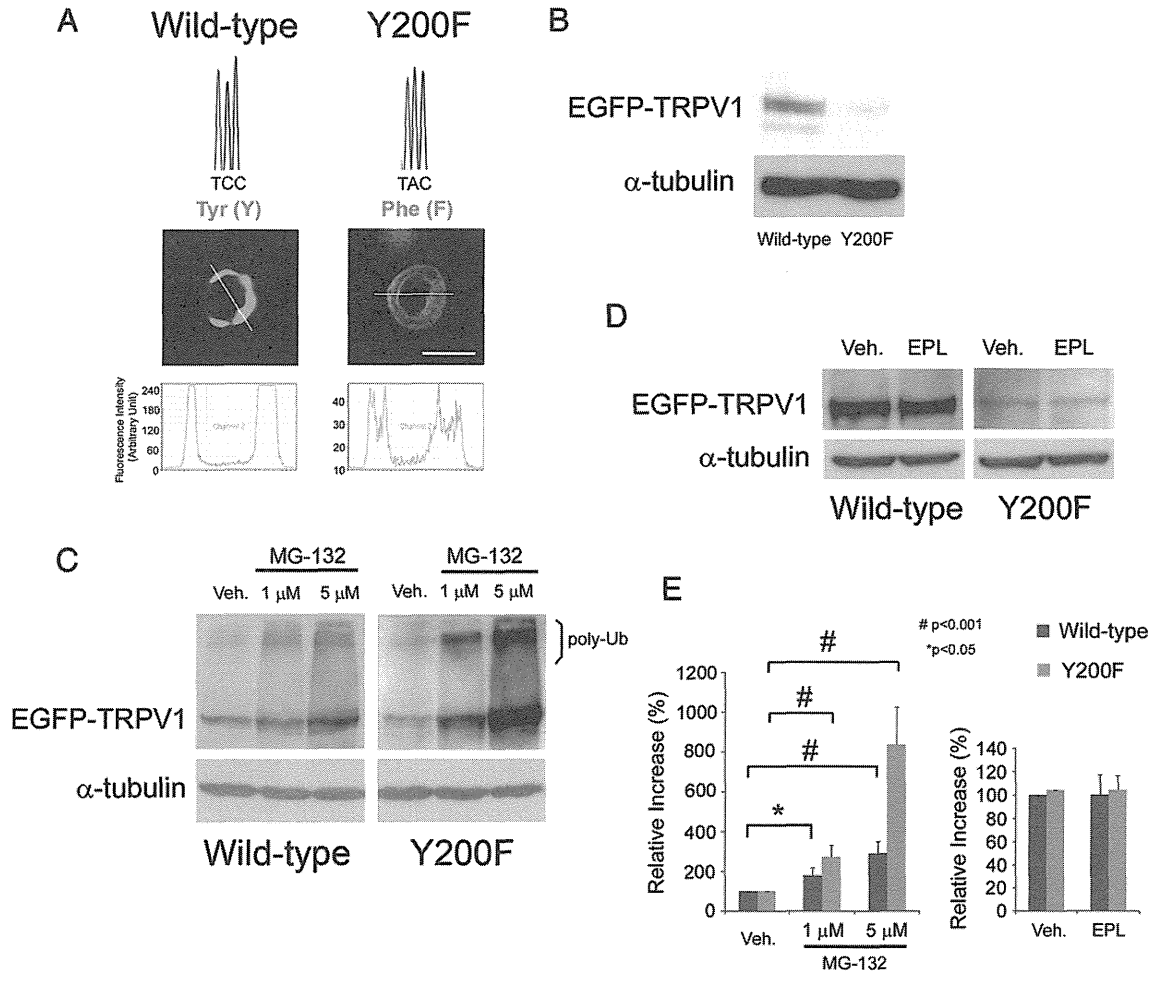

Fig. 8. Failure of TRPV1 to translocate to the plasma membrane led to proteasomal degradation. (A) EGFP-tagged wild-type and Y200F-mutant TRPV1 were transfected into PC12 cells. EGFP-tagged wild-type TRPV1 was primarily localized in the plasma membrane. The Y200F mutation, confirmed by DNA sequencing, resulted in altered localization; the EGFP-tagged Y200F TRPV1 mutant was diffusely present in the cytoplasm. As the GFP signal emitted by the Y200F-mutant was weak, a longer exposure condition was adopted when the image of this Y200F-expressing cell was acquired. Scale bar: 10 μm. GFP signal quantification along the thin white lines revealed that the GFP signal in the plasma membrane (~250 arbitrary units [AU]) was more intense than that in the cytoplasm (~50 AU). The analysis was carried out using Leica LAS AF software. (B) Western blot analysis showed that the steady-state expression level of Y200F-mutant TRPV1 was lower than that of wild-type TRPV1. (C) Proteasomal inhibition using MG-132 (1 and 5 μM; Sigma) led to increased expression of both wild-type and Y200F-mutated EGFP–TRPV1 in a dose-dependent manner. The magnitude of the elevation in MG-132-induced expression was greater in PC12 cells expressing Y200F-mutant TRPV1, indicating that cytoplasm-localized TRPV1 was more vulnerable to proteasomal degradation than was membrane-localized TRPV1. (D) Lysosomal protease inhibition with a combination of E64d (30 μM; Peptide Institute, Osaka, Japan), pepstatin A (15 μM; Peptide Institute), and leupeptin (20 μM; Peptide Institute) did not alter the expression of wild-type or Y200F-mutant TRPV1. EPL: E64d + pepstatin A + leupeptin. (E) Quantification of wild-type and Y200F-mutant EGFP–TRPV1 protein level alterations following proteasome and lysosomal protease inhibition.

TRPV1 is mediated by the sequential activation of phosphatidylinositol 3-kinase (PI3-K) and Src kinase (Stein et al., 2006; Zhang et al., 2005; Zhu and Oxford, 2007). Protein kinase C (PKC) also plays an important role in NGF-driven, exocytosis-mediated TRPV1 surface membrane expression, and the PKCδ-specific inhibitor rottlerin has been shown to inhibit NGF-dependent phosphorylation and functional potentiation of TRPV1, implying that PKC, particularly PKCδ, acts upstream of the Src kinase (Bhave et al., 2003; Bonnington and McNaughton, 2003; Morenilla-Palao et al., 2004; Zhang et al., 2005). This is supported by the finding that angiotensin-induced Src phosphorylation was abrogated by rottlerin in rat liver endothelial cells. Collectively, these results suggest that the role of PKCδ in TRPV1 Y200 phosphorylation appears likely to be mediated by Src kinase activation (Shah and Catt, 2002). Regulated exocytosis is accomplished when vesicles fuse with the plasma membrane due to the coordinated actions of SNARE proteins (Dolly et al., 2009; Südhof and Rothman, 2009). Recently, Camprubí-Robles et al. (2009) demonstrated that a lipopeptide that specifically inhibits SNAP25 activity attenuated NGF-induced TRPV1 trafficking to the plasma membrane (Camprubí-Robles et al., 2009), suggesting that Y200 phosphorylation is closely associated with TRPV1 mobilization by BoNT-A-sensitive exocytosis. Furthermore, a yeast two-hybrid study revealed that the N-terminal domain of TRPV1, including the Y200 residue, can interact with Snapin and synaptotagmin IX (Syt IX), which are both vesicular proteins related to exocytosis. Therefore, we reasoned that our results from Y200F-mutant TRPV1-expressing PC12 cells are pertinent to our in vivo findings regarding BoNT-A action.

The present study demonstrated the differential effect of BoNT-A on the trafficking of TRPV1 over $P2X_3$ in the TG neurons. Contrary to our finding, Apostolidis et al. (2005) reported concomitant decreases of TRPV1 and $P2X_3$ in the suburothelial nerve fibers after intradetrusor injections of BoNT-A in humans (Apostolidis et al., 2005). This discrepancy may reflect differences in tissues and/or species examined. Along with TRPV1, $P2X_3$ also plays an important role in the nociception of the trigeminal system (Shinoda et al., 2007, 2008; Staikopoulos et al., 2007). Hsieh et al. reported that the potent TRPV1 agonist, resiniferatoxin (RTX), induced degeneration of TRPV1-positive neuron in the dorsal root ganglia (DRG), followed by an increase in $P2X_3$ expression in the remaining DRG neurons. The number of $P2X_3$-positive neurons correlated with the magnitude of sensitization that developed after the RTX treatment. Their finding implies that $P2X_3$ expression

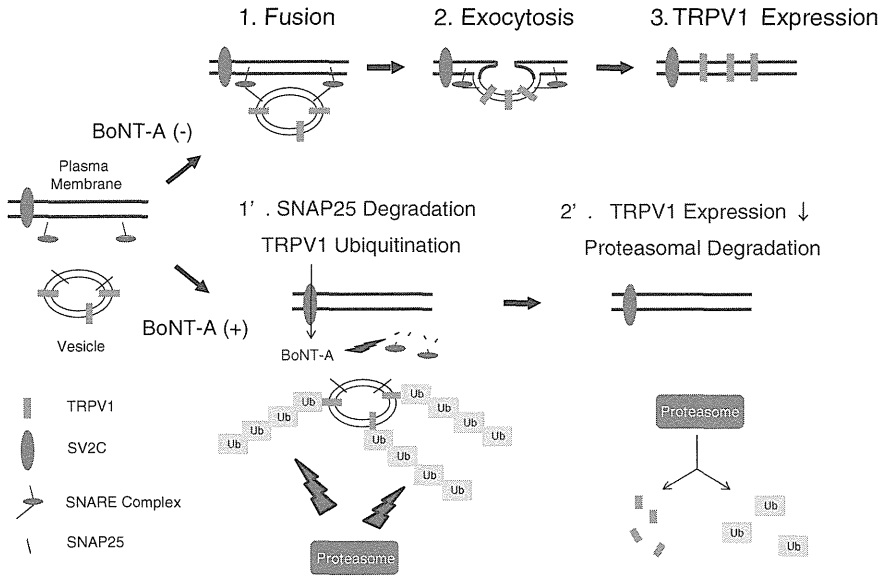

Fig. 9. Schematic model of intracellular events associated with the mechanism whereby BoNT-A reduces TRPV1 expression. TRPV1 plasma membrane expression is accomplished by regulated exocytosis. Under appropriate circumstances, TRPV1-carrying vesicles fuse with the plasma membrane (1). The ensuing exocytosis leads to plasma membrane surface expression of TRPV1, which is dependent on the coordinated actions of the SNARE complex (2, 3). In the presence of BoNT-A, which enters the cell through its acceptor protein, SV2C, SNAP25 is cleaved by the protease activity of BoNT-A (1′) (Dong et al., 2006), which inhibits exocytosis. The failure of TRPV1 to translocate to the plasma membrane renders TRPV1 vulnerable to ubiquitination and subsequent proteasomal degradation, thus resulting in decreased TRPV1 levels (2′).

increased in primary sensory neurons to compensate for the decreased TRPV1 expression. In this sense, in addition to BoNT-A administration, a therapeutic measure that controls $P2X_3$ expression level may be required to alleviate pain disorders.

The present study provides novel evidence that TRPV1 is susceptible to proteasomal degradation in the cytoplasm, unless it translocates to the plasma membrane. Proper cell surface receptor regulation is very important for various physiological functions. As wild-type TRPV1 was also shown to be sensitive to 24-hour-long MG132 treatment (Fig. 6C), proteasome-regulated TRPV1 turnover appears to be dynamic and is probably related to the fine-tuning of nociception. In this regard, the balance between neuronal receptor synthesis and degradation is expected to be tightly regulated. The ubiquitin-proteasome system is known to be involved in receptor catabolism. For example, NR1, an NMDA receptor subunit, is ubiquitinated by the F-box protein, Fbx2, a component of E3 ligase, and is then degraded by a proteasome (Kato et al., 2005). Details regarding the TRPV1 ubiquitination mechanism, including the identification of the responsible E3 ligase, remain to be elucidated. Nonetheless, it is a significant discovery of this study that blocking TRPV1 trafficking to the plasma membrane markedly decreases total TRPV1 expression due to proteasomal degradation. This finding provides important insight into therapeutic measures against pathological conditions in which total TRPV1 expression and recruitment to the plasma membrane are increased, as seen in inflammation-induced hyperalgesic states. Our results also revealed that there is no discernible contribution of lysosomal proteases to TRPV1 degradation.

This study provides a novel molecular basis for the efficacy of BoNT-A in the treatment of pain disorders. Previously, Gazerani et al. (2009) demonstrated that subcutaneous BoNT-A administered to the forehead reduced capsaicin-induced trigeminal pain in humans, thus providing strong evidence for a link between BoNT-A and TRPV1 in the human trigeminal system (Gazerani et al., 2009). The results of the rat pain behavior assay supported these findings and revealed the selectivity of the antinociceptive action of BoNT-A against TRPV1. In addition, the failure of BoNT-A pretreatment to affect $P2X_3$-mediated nocifensive behaviors made it unlikely that the molecular functions implicated in pain signal conduction and transmission, such as ion channels and neuronal receptors, were influenced by BoNT-A administration. Any detailed analysis of BoNT-A-induced molecular events has been impossible using only in vivo studies; therefore, the mechanism by which BoNT-A attenuated TRPV1 functions has remained unclear. Here, we demonstrated that local administration of BoNT-A to the face can target TG neurons of the ophthalmic division, including those receiving projections from the dura mater, and these neurons are related to nociception associated with headaches. Thus, these findings have clinical implications for headache disorders. Infectious and granulomatous diseases often affect meninges, and resultant meningitis causes severe pain that is refractory to conventional therapy. TRPV1 channel blockers have been used in humans for the therapeutic purpose (Meents et al., 2010). Among them, AMG 517, a highly TRPV1 selective antagonist, was administered to alleviate pain after molar extraction, which caused long-lasting hyperthermia with maximal body temperature above 40 °C (Gavva et al., 2008). This is consistent with the body temperature-regulating function of TRPV1 (Romanovsky et al., 2009), and the unfavorable side-effect hampers the further clinical application of this agent. BoNT-A-mediated inhibition of intracellular TRPV1 trafficking seems to be superior to TRPV1 channel blockage with respect to the development of hyperthermia.

BoNT-A has been demonstrated to be effective for chronic migraine (Aurora et al., 2010; Diener et al., 2010). Although the precise pathophysiology of migraine is still largely unknown, some researchers postulate that neurogenic inflammation in the dura mater plays an important role in the generation of migraine pain (Moskowitz, 1984). Following this line, long-term inflammation likely causes TRPV1 upregulation in the trigeminal nociceptors and may be involved in chronic migraine pathophysiology; the efficaciousness of BoNT-A against chronic migraine seems consistent with this hypothesis. Ideally, oral drugs capable of regulating exocytosis-mediated TRPV1 plasma membrane trafficking should be developed. Such drugs could be expected to have a broad spectrum of clinical applications, including the treatment of a variety of non-neurological disorders associated with TRPV1 hyperactivity, such as respiratory tract hypersensitivity (Lee and Gu, 2009) and inflammatory bowel diseases (Akbar et al., 2010).

Acknowledgments

This research was supported in part by a Grant-in-Aid for Scientific Research (grant number 22390182 to N. Suzuki) from the Ministry of Education, Culture, Sports, Science and Technology of Japan and an AstraZeneca Research Grant (to M. Shibata).

References

Akbar, A., Yiangou, Y., Facer, P., Brydon, W.G., Walters, J.R., Anand, P., Ghosh, S., 2010. Expression of the TRPV1 receptor differs in quiescent inflammatory bowel disease with or without abdominal pain. Gut 59, 767–774.

Antonucci, F., Rossi, C., Gianfranceschi, L., Rossetto, O., Caleo, M., 2008. Long-distance retrograde effects of botulinum neurotoxin A. J. Neurosci. 28, 3689–3696.

Apostolidis, A., Popat, R., Yiangou, Y., Cockayne, D., Ford, A.P., Davis, J.B., Dasgupta, P., Fowler, C.J., Anand, P., 2005. Decreased sensory receptors P2X3 and TRPV1 in suburothelial nerve fibers following intradetrusor injections of botulinum toxin for human detrusor overactivity. J. Urol. 174, 977–982 (discussion 982-3).

Aurora, S.K., Dodick, D.W., Turkel, C.C., DeGryse, R.E., Silberstein, S.D., Lipton, R.B., Diener, H.C., Brin, M.F., 2010. OnabotulinumtoxinA for treatment of chronic migraine: results from the double-blind, randomized, placebo-controlled phase of the PREEMPT 1 trial. Cephalalgia 30, 793–803.

Bhave, G., Hu, H.J., Glauner, K.S., Zhu, W., Wang, H., Brasier, D.J., Oxford, G.S., Gereau, R.W.T., 2003. Protein kinase C phosphorylation sensitizes but does not activate the capsaicin receptor transient receptor potential vanilloid 1 (TRPV1). Proc. Natl. Acad. Sci. U. S. A. 100, 12480–12485.

Bonnington, J.K., McNaughton, P.A., 2003. Signalling pathways involved in the sensitisation of mouse nociceptive neurones by nerve growth factor. J. Physiol. 551, 433–446.

Camprubí-Robles, M., Planells-Cases, R., Ferrer-Montiel, A., 2009. Differential contribution of SNARE-dependent exocytosis to inflammatory potentiation of TRPV1 in nociceptors. FASEB J. 23, 3722–3733.

Caterina, M.J., Leffler, A., Malmberg, A.B., Martin, W.J., Trafton, J., Petersen-Zeitz, K.R., Koltzenburg, M., Basbaum, A.I., Julius, D., 2000. Impaired nociception and pain sensation in mice lacking the capsaicin receptor. Science 288, 306–313.

Diener, H.C., Dodick, D.W., Aurora, S.K., Turkel, C.C., DeGryse, R.E., Lipton, R.B., Silberstein, S.D., Brin, M.F., 2010. OnabotulinumtoxinA for treatment of chronic migraine: results from the double-blind, randomized, placebo-controlled phase of the PREEMPT 2 trial. Cephalalgia 30, 804–814.

Dolly, J.O., Lawrence, G.W., Meng, J., Wang, J., Ovsepian, S.V., 2009. Neuro-exocytosis: botulinum toxins as inhibitory probes and versatile therapeutics. Curr. Opin. Pharmacol. 9, 326–335.

Dong, M., Yeh, F., Tepp, W.H., Dean, C., Johnson, E.A., Janz, R., Chapman, E.R., 2006. SV2 is the protein receptor for botulinum neurotoxin A. Science 312, 592–596.

Gavva, N.R., Treanor, J.J., Garami, A., Fang, L., Surapaneni, S., Akrami, A., Alvarez, F., Bak, A., Darling, M., Gore, A., Jang, G.R., Kesslak, J.P., Ni, L., Norman, M.H., Palluconi, G., Rose, M.J., Salfi, M., Tan, E., Romanovsky, A.A., Banfield, C., Davar, G., 2008. Pharmacological blockade of the vanilloid receptor TRPV1 elicits marked hyperthermia in humans. Pain 136, 202–210.

Gazerani, P., Pedersen, N.S., Staahl, C., Drewes, A.M., Arendt-Nielsen, L., 2009. Subcutaneous Botulinum toxin type A reduces capsaicin-induced trigeminal pain and vasomotor reactions in human skin. Pain 141, 60–69.

Goldberg, A.L., 2003. Protein degradation and protection against misfolded or damaged proteins. Nature 426, 895–899.

Gunthorpe, M.J., Chizh, B.A., 2009. Clinical development of TRPV1 antagonists: targeting a pivotal point in the pain pathway. Drug Discov. Today 14, 56–67.

Honda, K., Kitagawa, J., Sessle, B.J., Kondo, M., Tsuboi, Y., Yonehara, Y., Iwata, K., 2008. Mechanisms involved in an increment of multimodal excitability of medullary and upper cervical dorsal horn neurons following cutaneous capsaicin treatment. Mol. Pain 4, 59.

Kato, A., Rouach, N., Nicoll, R.A., Bredt, D.S., 2005. Activity-dependent NMDA receptor degradation mediated by retrotranslocation and ubiquitination. Proc. Natl. Acad. Sci. U. S. A. 102, 5600–5605.

Kitamura, Y., Matsuka, Y., Spigelman, I., Ishihara, Y., Yamamoto, Y., Sonoyama, W., Kamioka, H., Yamashiro, T., Kuboki, T., Oguma, K., 2009. Botulinum toxin type a (150 kDa) decreases exaggerated neurotransmitter release from trigeminal ganglion neurons and relieves neuropathy behaviors induced by infraorbital nerve constriction. Neuroscience 159, 1422–1429.

Lee, L.Y., Gu, Q., 2009. Role of TRPV1 in inflammation-induced airway hypersensitivity. Curr. Opin. Pharmacol. 9, 243–249.

Lim, E.C., Seet, R.C., 2010. Use of botulinum toxin in the neurology clinic. Nat. Rev. Neurol. 6, 624–636.

Matak, I., Bach-Rojecky, L., Filipovic, B., Lackovic, Z., 2011. Behavioral and immunohistochemical evidence for central antinociceptive activity of botulinum toxin A. Neuroscience 186, 201–207.

Meents, J.E., Neeb, L., Reuter, U., 2010. TRPV1 in migraine pathophysiology. Trends Mol. Med. 16, 153–159.

Meng, J., Wang, J., Lawrence, G., Dolly, J.O., 2007. Synaptobrevin I mediates exocytosis of CGRP from sensory neurons and inhibition by botulinum toxins reflects their anti-nociceptive potential. J. Cell Sci. 120, 2864–2874.

Mizushima, N., Yoshimori, T., Levine, B., 2010. Methods in mammalian autophagy research. Cell 140, 313–326.

Morenilla-Palao, C., Planells-Cases, R., García-Sanz, N., Ferrer-Montiel, A., 2004. Regulated exocytosis contributes to protein kinase C potentiation of vanilloid receptor activity. J. Biol. Chem. 279, 25665–25672.

Moskowitz, M.A., 1984. The neurobiology of vascular head pain. Ann. Neurol. 16, 157–168.

Naumann, M., So, Y., Argoff, C.E., Childers, M.K., Dykstra, D.D., Gronseth, G.S., Jabbari, B., Kaufmann, H.C., Schurch, B., Silberstein, S.D., Simpson, D.M., 2008. Assessment: Botulinum neurotoxin in the treatment of autonomic disorders and pain (an evidence-based review): report of the Therapeutics and Technology Assessment Subcommittee of the American Academy of Neurology. Neurology 70, 1707–1714.

Romanovsky, A.A., Almeida, M.C., Garami, A., Steiner, A.A., Norman, M.H., Morrison, S.F., Nakamura, K., Burmeister, J.J., Nucci, T.B., 2009. The transient receptor potential vanilloid-1 channel in thermoregulation: a thermosensor it is not. Pharmacol. Rev. 61, 228–261.

Südhof, T.C., Rothman, J.E., 2009. Membrane fusion: grappling with SNARE and SM proteins. Science 323, 474–477.

Shah, B.H., Catt, K.J., 2002. Calcium-independent activation of extracellularly regulated kinases 1 and 2 by angiotensin II in hepatic C9 cells: roles of protein kinase Cdelta, Src/proline-rich tyrosine kinase 2, and epidermal growth receptor trans-activation. Mol. Pharmacol. 61, 343–351.

Shimada, S.G., LaMotte, R.H., 2008. Behavioral differentiation between itch and pain in mouse. Pain 139, 681–687.

Shimizu, T., Toriumi, H., Sato, H., Shibata, M., Nagata, E., Gotoh, K., Suzuki, N., 2007. Distribution and origin of TRPV1 receptor-containing nerve fibers in the dura mater of rat. Brain Res. 1173, 84–91.

Shinoda, M., Kawashima, K., Ozaki, N., Asai, H., Nagamine, K., Sugiura, Y., 2007. P2X3 receptor mediates heat hyperalgesia in a rat model of trigeminal neuropathic pain. J. Pain 8, 588–597.

Shinoda, M., Ozaki, N., Sugiura, Y., 2008. Involvement of ATP and its receptors on nociception in rat model of masseter muscle pain. Pain 134, 148–157.

Staikopoulos, V., Sessle, B.J., Furness, J.B., Jennings, E.A., 2007. Localization of P2X2 and P2X3 receptors in rat trigeminal ganglion neurons. Neuroscience 144, 208–216.

Stein, A.T., Ufret-Vincenty, C.A., Hua, L., Santana, L.F., Gordon, S.E., 2006. Phosphoinositide 3-kinase binds to TRPV1 and mediates NGF-stimulated TRPV1 trafficking to the plasma membrane. J. Gen. Physiol. 128, 509–522.

Szallasi, A., Cruz, F., Geppetti, P., 2006. TRPV1: a therapeutic target for novel analgesic drugs? Trends Mol. Med. 12, 545–554.

Van Buren, J.J., Bhat, S., Rotello, R., Pauza, M.E., Premkumar, L.S., 2005. Sensitization and translocation of TRPV1 by insulin and IGF-I. Mol. Pain 1, 17.

Zhang, X., Huang, J., McNaughton, P.A., 2005. NGF rapidly increases membrane expression of TRPV1 heat-gated ion channels. EMBO J. 24, 4211–4223.

Zhu, W., Oxford, G.S., 2007. Phosphoinositide-3-kinase and mitogen activated protein kinase signaling pathways mediate acute NGF sensitization of TRPV1. Mol. Cell. Neurosci. 34, 689–700.

Alterations in microglia and astrocytes in the trigeminal nucleus caudalis by repetitive TRPV1 stimulation on the trigeminal nociceptors

Toshiya Kuroi, Toshihiko Shimizu, Mamoru Shibata, Haruki Toriumi, Megumi Funakubo, Tatsuo Iwashita, Hitoshi Sato, Kenzo Koizumi and Norihiro Suzuki

TRPV1 is a nonselective cation channel in nociceptors. TRPV1 stimulation has been shown to lead to the activation of microglia and astrocytes in the dorsal horn of the spinal cord. However, information on the effect of TRPV1 stimulation on glial activation in the trigeminal nucleus caudalis (TNC) is lacking. Here, we stimulated TRPV1 in the trigeminal afferents by a repetitive injection of 10 mmol/l capsaicin into the whisker pad for 2 days (d2 group), 4 days (d4 group), or 6 days (d6 group). As a control (c group), the vehicle was injected for 2 days. Anti-Iba1 and anti-glial fibrillary acidic protein antibodies were used to immunostain microglia and astrocytes in the TNC, respectively. The ratio of the cross-sectional area immunoreactive for Iba1 to the entire area of the TNC was increased in the d2 group compared with the c group on the injected side. Microglia were recruited to the superficial layers of the TNC. The numbers of microglia were reduced in the d4 group and the d6 group compared with the d2 group. The ratio of the cross-sectional area immunoreactive for glial fibrillary acidic protein to the entire TNC showed a significant increase in d2 group and the d4 group compared with the c group on the injected side. Behavioral analysis indicated that mechanical allodynia began to develop after 2 days of capsaicin treatment and persisted for at least 6 days after the onset of the repetitive capsaicin injection. These data indicate that TRPV1 stimulation activates the microglia and astrocytes in temporally distinct ways and that the development of mechanical allodynia is independent of such glial activation. *NeuroReport* 23:560–565 © 2012 Wolters Kluwer Health | Lippincott Williams & Wilkins.

NeuroReport 2012, 23:560–565

Keywords: astrocyte, mechanical allodynia, microglia, trigeminal nucleus caudalis, TRPV1

Department of Neurology, School of Medicine, Keio University, Tokyo, Japan

Correspondence to Mamoru Shibata, MD, PhD, Department of Neurology, School of Medicine, Keio University, 35 Shinanomachi, Shinjuku-ku, Tokyo 160-8582, Japan
Tel: +81 3 5363 3788; fax: +81 3 3353 1272;
e-mail: mshibata@a7.keio.jp

Received 26 March 2012 accepted 2 April 2012

Introduction

Glial cells are known to play a vital role in chronic pain. Several studies have shown the activation of the microglia and astrocytes in the spinal cord after inflammatory tissue damage [1,2] or a peripheral nerve injury [3,4]. The transient receptor potential, subfamily V, member 1 (TRPV1) receptor is a capsaicin-sensitive, proton-sensitive, and heat-sensitive nonselective cation channel and plays a role in nociception [5]. There are several inflammatory diseases involving the trigeminal nerve-innervated areas that cause severe and intractable pain, as exemplified by meningitis and pulpitis. As TRPV1 function is known to be upregulated by inflammatory mediators, the cation channel plays a pivotal role in the evolution of inflammatory pain. Although the precise relationship between nociceptive stimulation and glial activation in the central nervous system remains unclear, recent evidence has shown TRPV1-mediated activation of spinal cord glial cells [6]. An intraplantar capsaicin injection induced thermal hypersensitivity, which was accompanied by an increase in immunostaining for glial markers in the dorsal horn. However, information on the relationship between TRPV1 stimulation and glial activation in the brainstem trigeminal nucleus region appears to be lacking.

In this study, we aim to observe the alterations in the microglia and astrocytes in the trigeminal nucleus caudalis (TNC) by a repetitive TRPV1 stimulation using immunohistochemical techniques and to determine the correlation between the immunohistological data and the development of nocifensive behaviors.

Materials and methods

Animals

Experiments were performed on male Sprague–Dawley rats ($n = 27$; body weight, 250–300 g), 12 of which were used for immunohistochemistry, with the remaining 15 used for behavioral testing. These experimental procedures were approved by the Animal Welfare Committee of Keio University (No. 08075). Furthermore, all the procedures were undertaken with the utmost care to minimize the suffering of the animals.

0959-4965 © 2012 Wolters Kluwer Health | Lippincott Williams & Wilkins DOI: 10.1097/WNR.0b013e3283546242

Drug administration

After deep anesthetization with halothane, either 100 µl of a 10 mmol/l 8-methyl-*N*-vanillyl-*trans*-6-nonenamide (capsaicin) solution (3.1 mg/ml in saline with 6% ethanol and 7% Tween-80; Sigma-Aldrich, St Louis, Missouri, USA) or a vehicle (saline with 6% ethanol and 7% Tween-80) was subcutaneously injected into the left whisker pad of each animal. In the immunohistochemical experiment, animals were divided into four groups ($n = 3$ in each group) as follows: rats treated with the vehicle for 2 days (c group), and with capsaicin for 2 days (d2 group), 4 days (d4 group), and 6 days (d6 group). In clinically important disease conditions, such as meningitis and pulpitis, nociceptive stimulation is present for a certain period. Therefore, we chose repetitive capsaicin treatment in this study to mimic clinical situations as in the inflammatory diseases.

Immunohistochemistry

On the day after the last injection in each group, the animals were deeply anesthetized and transcardially perfused with a mixture of 2% formaldehyde and 0.2% picric acid in 0.1 mol/l phosphate buffer (pH 7.0). Immediately after the perfusion fixation, the brainstem was dissected out and the portion harboring the TNC was processed into frozen serial sections of 12 µm thickness using a cryostat (Reichert-Jung Cryocut 1800; Leica Instruments, Buffalo Grove, Illinois, USA). The first ones of three consecutive sections were used for immunostaining. The frozen sections were preincubated with 10% normal donkey serum for 30 min. The sections were incubated with primary antibodies for 48 h at room temperature. The sections were then rinsed with 0.01 mol/l PBS and incubated with species-specific secondary antibodies for 2 h at room temperature. The specimens were mounted in buffered glycerol (pH 8.6). In this manner, the slides were double labeled with the anti-ionizing calcium-binding adapter molecule 1 (Iba1) antibody (raised in rabbits; code 019-19741; Wako Chemicals, Osaka, Japan; 1:200) and the anti-glial fibrillary acidic protein (GFAP) antibody (raised in mice; code G3893; Sigma-Aldrich; 1:500). Immunoreactivities with the primary antibodies were visualized with species-specific secondary antibodies raised in donkeys and conjugated to Cy3 or fluorescein isothiocyanate; all the antibodies were obtained from Jackson Immunoresearch Laboratories (West Grove, Pennsylvania, USA).

The immunolabeled specimens were examined under a Keyence BIOREVO BZ-9000 microscope (Keyence, Osaka, Japan) fitted with a highly discriminating filter.

Quantitative analysis of immunoreactivities for glial cells

We chose eight brainstem sections at the level of the TNC on the capsaicin-injected side in each animal (three animals per group). The sections were immunostained for Iba1 and GFAP to label the microglia and the astrocytes, respectively. Digital images were obtained using a high-quality CCD camera attached to a fluorescent microscope (BIOREVO BZ-9000; Keyence) and saved as Tiff files. The TNC area on the section images was determined according to the method of Paxinos and Watson [7]. Subsequently, we calculated the ratio of cross-sectional area immunoreactive for Iba1 or GFAP within the TNC area and estimated the number of Iba1-immunoreactivity (IR) cells per 1 mm^2 of the TNC area using an image analysis software (Keyence). In these quantitative analyses, we applied an identical fluorescence excitation condition to all of the sections examined. All enhancements were made uniformly across entire images. For capturing fluorescence signals representing immunoreactivities for Iba1 and GFAP, we used a distinct optimal condition for each marker in terms of segregation and threshold settings.

Data were presented as mean ± SD. Differences among the groups were assessed by one-way analysis of variance, followed by individual post-hoc comparisons (Bonferroni's test), and P value less than 0.05 was considered significant (SPSS for Windows, version 19; SPSS Inc., Chicago, Illinois, USA).

Behavioral testing

Pain-related behaviors were induced by mechanical stimulation using home-made von Frey hairs (VFHs; diameter 0.5 mm; bending forces 34.3 mN). Rats were allowed to acclimate to their surroundings for 30 min before testing. During the procedure for assessment of sensitivity to mechanical stimuli, animals were restrained at the trunk with a towel to calm them and treated gently. Each VFH was applied ten times (once every 10 s) to the lateral facial skin, and the number of wiping instances by forelimb or withdrawal response was then counted [8]. The frequency of nocifensive behaviors (head withdrawal or wiping by the forelimb) was measured in 10 trials. Animals were subjected to the behavioral test on two occasions: before the injection [1 day before injection (pre 2)] and just before the first injection (pre 1). Subsequently, 10 mmol/l capsaicin (100 µl) was injected into the left whisker pad. The same injection procedure was repeated once a day for the designated period. Before each injection procedure, the behavioral test was carried out. In the control animals, mechanical sensitivity was assessed using the same protocol without the administration of capsaicin. All the behavioral tests were carried out by an examiner blinded to the identity of the animals.

Data were presented as mean ± SD. Differences between groups were evaluated by one-way analysis of variance, followed by individual post-hoc comparisons (Bonferroni's test), and P value less than 0.05 was considered significant.

Fig. 1

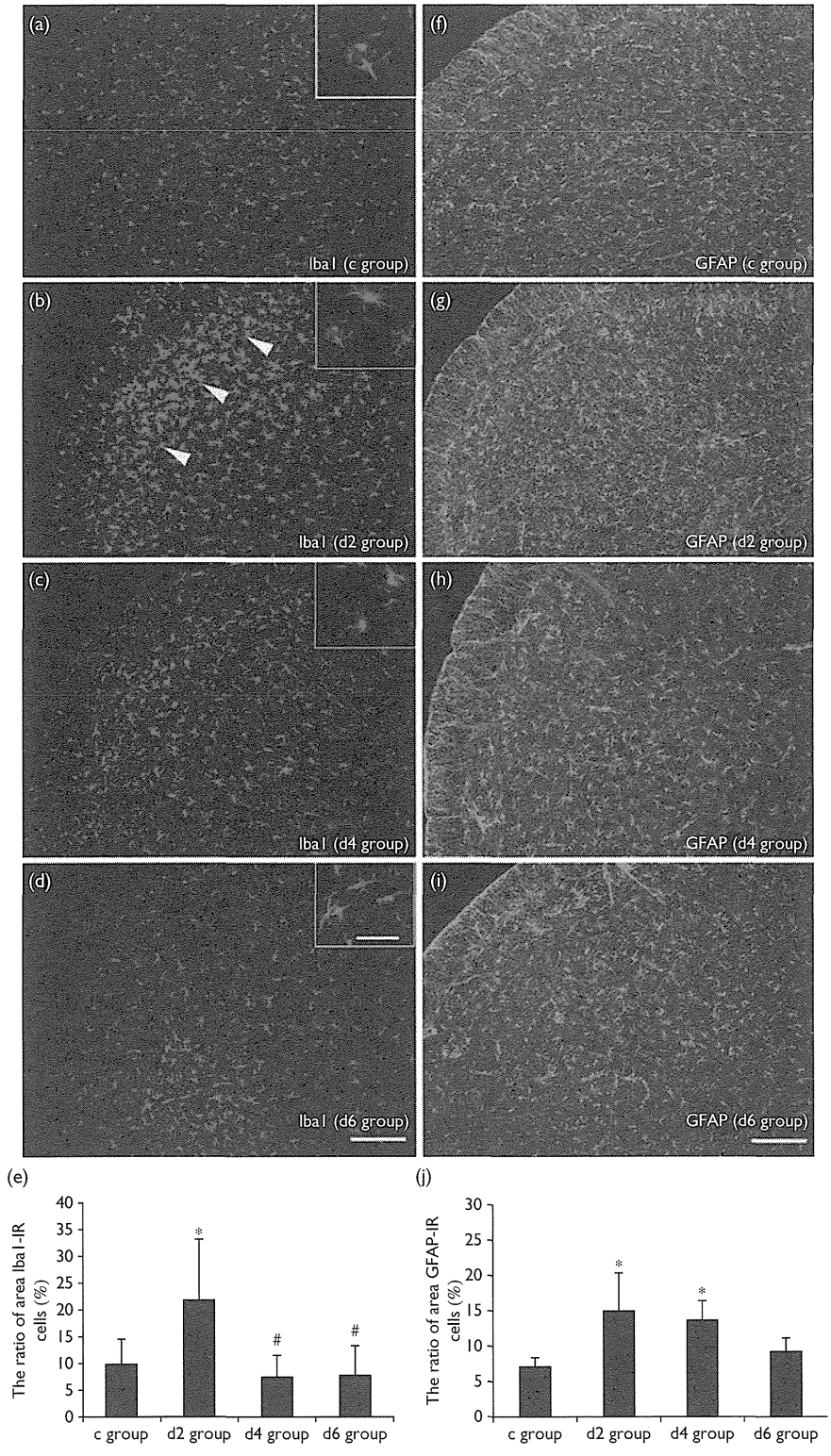

Alterations in Iba1 (a–d) and glial fibrillary acidic protein (GFAP) (f–i) expressions in the ipsilateral trigeminal nucleus caudalis (TNC) by a repetitive capsaicin injection into the whisker pad. Vehicle injection for 2 days (a, f). Capsaicin injection for 2 days (b, g). Arrowheads indicate the superficial laminae of TNC. Capsaicin injection for 4 days (c, h). Capsaicin injection for 6 days (d, i). The scale bars = 200 μm. Enlargements in the insets show the alterations in the morphology of microglia. The scale bar in the inset = 50 μm. Quantitative analysis of Iba1-immunoreactivity (IR) cells and GFAP-IR cells (e, j). The ratio of area immunoreactive for Iba1 (e) and GFAP (j) to the total area of the ipsilateral TNC (a–i). The bars show the mean ± SD. *$P < 0.05$ versus c group. #$P < 0.05$ versus d2 group.

Results

Effect of trigeminal nociceptive stimulation on Iba1 and glial fibrillary acidic protein immunoreactivity in the trigeminal nucleus caudalis

As shown in Fig. 1a, Iba1-IR was observed sparsely in the TNC in the c group. However, after trigeminal capsaicin stimulation, Iba1-IR was increased especially in the superficial laminae of TNC, where the central axons of trigeminal ganglion neurons make synaptic contact with the second-order trigeminal neurons, in the d2 group (Fig. 1b, arrowheads). In addition, marked hypertrophy of Iba1-IR cells was observed in the d2 group (Fig. 1b, inset). Morphologically, the majority of the hypertrophic microglia appeared to be ramified microglia, and only a few ameboid microglia were identified. There were fewer Iba1-IR cells and the extent of hypertrophy was less conspicuous in the d4 group and the d6 group as compared with the d2 group (Fig. 1c and d). Quantitatively, the ratio of the cross-sectional area of Iba1-IR cells to the TNC area was 9.9±4.7% in the c group, 23.7±11.4% in the d2 group, 7.4±4.1% in the d4 group, and 7.8±5.6% in the d6 group (mean±SD; Fig. 1e). There was a significant difference between the d2 group and the c group ($P < 0.05$). Also, the estimated numbers of Iba1-IR cells within the TNC region were 438.0±124.9/mm^2 in the c group, 511.8±139.8/mm^2 in the d2 group, 292.4±109.0/mm^2 in the d4 group, and 286.2±117.3/mm^2 in the d6 group (mean±SD; Fig. 2). The estimated numbers in the d4 group and the d6 group were significantly decreased, compared with the d2 group ($P < 0.05$). The alterations in GFAP-IR in TNC after capsaicin injections showed a temporal profile distinct from those of Iba1-IR. As shown in Fig. 1f, GFAP-IR was observed in the TNC before capsaicin stimulation in the c group. The IR of GFAP cells was also increased in the capsaicin injection groups (Fig. 1g–i), which was accompanied by cytoplasmic hypertrophy. However, there was a trend toward reversion to the basal level in the d6 group (Fig. 1i).

The ratio of the cross-sectional area of GFAP-IR cells to the TNC area was 7.3±1.2% in the c group, 15.1±5.4% in the d2 group, 13.8±2.7% in the d4 group, and 9.3±1.9% in the d6 group (mean±SD; Fig. 1j). There was a significant increase in the d2 group and the d4 group compared with the c group ($P < 0.05$). The number of GFAP-IR cells was not calculated in this study because of technical difficulty in the precise counting of these cells.

Effects of trigeminal nociceptive stimulation on nocifensive behaviors

As shown in Fig. 3, the VFH stimulation procedure that we utilized did not induce a nocifensive response before trigeminal capsaicin stimulation (Fig. 3, pre 1 and pre 2). However, after the repetitive administration of capsaicin, the number of nocifensive responses increased gradually (day 1, 1.5±1.2 [mean±SD] times; day 2, 2.3±1.5 times; day 3, 2.8±1.7 times; day 4, 2.8±0.6 times; day 5, 4.1±1.3 times; day 6, 3.4±1.0 times) and the maximal number of nocifensive responses was observed on day 5. The number of nocifensive responses was significantly increased on days 2, 3, 4, 5, and 6 compared with pre 1 and pre 2. Meanwhile, the control animals did not show a significant change in the nocifensive responses during the observation period. Significant differences ($P < 0.05$) were found between the capsaicin-treated animals and the control animals at days 4, 5, and 6 (day 4, 0.5±0.8 times; day 5, 0.8±0.8 times; and day 6, 1.0±1.1 times).

Fig. 2

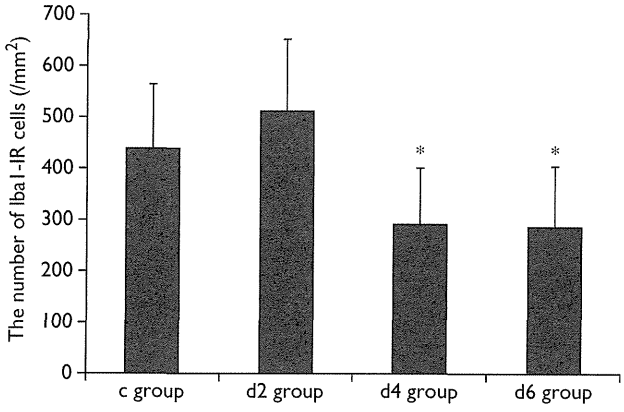

Quantitative analysis of Iba1-immunoreactivity (IR) cells per 1 mm^2 area of the ipsilateral trigeminal nucleus caudalis. The bars show the mean ± SD. *P<0.05 versus d2 group.

Fig. 3

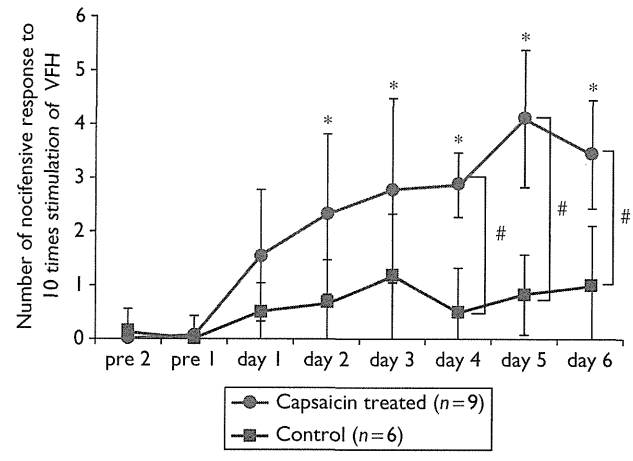

Nocifensive responses to mechanical stimulation to the ipsilateral face using von Frey hair (VFH). The bars represent the mean ± SD. *P<0.05 versus pre 1 and 2. #P<0.05 capsaicin-treated versus control.

Discussion

The present study showed that repetitive TRPV1 stimulation at trigeminal nociceptors induced transient morphological alterations in the microglia and astrocytes in the TNC. Both microglia and astrocytes showed cytoplasmic hypertrophy and, consequently, the areas immunoreactive for their markers, Iba1 and GFAP, increased after TRPV1 stimulation. Such changes were the most conspicuous at day 2, after which immunoreactivities for both markers gradually became less marked. At day 2, microglia were recruited to superficial layers of the TNC, where the first-order trigeminal neurons make synaptic contact with the second-order neurons. The number of microglia was reduced after day 2. Furthermore, our data indicated a temporal discrepancy between the glial morphological alterations and the occurrence of mechanical allodynia. Several lines of evidence have indicated that glial cell activation is responsible for the induction of mechanical allodynia in neuropathic pain models [9,10]. In response to a nerve injury, microglia have been shown to be rapidly activated and involved in the initiation of chronic pain. Meanwhile, astrocytes are activated on a slower timeline, and are involved in the maintenance of chronic pain [11,12]. Hence, the present study has shown a novel pattern of glial activation, apparently irrelevant to the development of mechanical allodynia.

Chen *et al.* [6] have previously reported that a single intraplantar injection of capsaicin induced hypertrophic changes in the microglia and astrocytes in the dorsal horn of the mouse lumbar spinal cord at day 3, but they did not provide any quantitative data for a longer time period. Despite the differences in animal species and experimental settings, the rapidly induced morphological changes after capsaicin treatment appear to be a common feature of glial cells irrespective of their locations in neural tissue.

Whether the activation of microglia and astrocytes is related to the development of mechanical allodynia is controversial. As mentioned above, most studies using neuropathic pain models support the role of glial activation in the occurrence of allodynia [9,10]. However, in inflammatory pain caused by complete Freund's adjuvant injection, mechanical allodynia has been shown to be induced in a manner independent of glial activation [13,14]. It is inferred that the mode of action of glial cells differs in accordance with the experimental settings. Glial cells in the central nervous system serve a number of housekeeping functions required for healthy neuronal communication [9]. Particularly, microglia are known to play a role in the maintenance of synaptic integrity. Morphologically, resting microglia are ramified and they dynamically extend and retract their processes for surveillance of the microenvironment [15]. In response to nerve injury and brain ischemia, activated microglia migrate to synapses and secrete neurotrophic factors capable of repairing neurons [16,17]. In our study, we observed that Iba1-IR cells were recruited to the superficial laminae of the TNC, where the central axons of trigeminal ganglion neurons make synaptic contact with the second-order trigeminal neurons. We did not observe any upregulation of IL-1β, P_2X4, or phosphorylated p38, which have been shown to contribute to neuronal damage [18–20] (data not shown). Moreover, there were only a few microglia with thick and retracted processes (ameboid microglia), which are associated with their neurotoxic actions [21]. Hence, it is likely that the activation of microglia by repetitive peripheral TRPV1 stimulation in this study was neuroprotective. The number of microglia located in the TNC decreased at days 4 and 6. Microglia may have exited from the TNC. Alternatively, they may have died through an apoptotic process. Activation-induced microglial apoptotic death has been reported in inflammatory and ischemic conditions [22,23]. Moreover, the decrease in neuroprotective microglia may have contributed toward the development of mechanical allodynia. Interestingly, TRPV1 knockout mice have a higher density of microglia and astrocytes in the spinal dorsal horn as compared with wild-type mice [6], which raises the possibility that there is a certain TRPV1-mediated machinery that decreases glial numbers. Our observations that glial cell numbers declined after 2 days of capsaicin treatment may reflect such a modulatory role of TRPV1.

Our results have provided a novel insight into the roles of brainstem glial cells under the TRPV1-relevant pathological pain conditions, which include meningitis, pulpitis, and possibly migraine.

Conclusion

In summary, we have shown the novel dynamics of glial activation in a TRPV1-associated pain model. TRPV1 induced a transient activation of glial cells in temporal profiles discrepant from the development of mechanical allodynia, and activated microglia appeared to exert protective effects on trigeminal synaptic functions.

Acknowledgements

This research was supported in part by a Grant-in-Aid for Scientific Research (Grant No. 22390182 to Norihiro Suzuki) from the Ministry of Education, Culture, Sports, Science and Technology of Japan, and a grant from the Takeda Science Foundation to Mamoru Shibata.

Conflicts of interest

There are no conflicts of interest.

References

1 Raghavendra V, Tanga FY, DeLeo JA. Complete Freund's adjuvant-induced peripheral inflammation evokes glial activation and proinflammatory cytokine expression in the CNS. *Eur J Neurosci* 2004; **20**:467–473.

2 Villa G, Ceruti S, Zanardelli M, Magni G, Jasmin L, Ohara PT Abbracchio MP. Temporomandibular joint inflammation activates glial and

immune cells in both the trigeminal ganglia and in the spinal trigeminal nucleus. *Mol Pain* 2010; **6**:89.
3 McMahon SB, Malcangio M. Current challenges in glia-pain biology. *Neuron* 2009; **64**:46–54.
4 Watkins LR, Maier SF. Beyond neurons: evidence that immune and glial cells contribute to pathological pain states. *Physiol Rev* 2002; **82**:981–1011.
5 Szallasi A, Cruz F, Geppetti P. TRPV1: a therapeutic target for novel analgesic drug? *Trends Mol Med* 2006; **12**:545–554.
6 Chen Y, Willcockson HH, Valtschanoff JG. Influence of the vanilloid receptor TRPV1 on the activation of spinal glia in mouse models of pain. *Exp Neurol* 2009; **220**:383–390.
7 Paxinos G, Watson C. *The rat brain in stereotaxic coordinate*. Orlando: Academic Press; 1998.
8 Shinoda M, Kawashima K, Ozaki N, Asai H, Nagamine K, Sugiura Y. P2X3 receptor mediates heat hyperalgesia in a rat model of trigeminal neuropathic pain. *J Pain* 2007; **8**:588–597.
9 Milligan ED, Watkins LR. Pathological and protective roles of glia in chronic pain. *Nat Rev Neurosci* 2009; **10**:23–36.
10 Benarroch EE. Central neuron-glia interactions and neuropathic pain: overview of recent concepts and clinical implications. *Neurology* 2011; **75**:273–278.
11 Romero-Sandoval A, Chai N, Nutile-McMenemy N, Deleo JA. A comparison of spinal Iba1 and GFAP expression in rodent models of acute and chronic pain. *Brain Res* 2008; **1219**:116–126.
12 Zhang J, De Koninck Y. Spatial and temporal relationship between monocyte chemoattractant protein-1 expression and spinal glial activation following peripheral nerve injury. *J Neurochem* 2006; **97**:772–783.
13 Clark AK, Gentry C, Bradbury EJ, McMahon SB, Malcangio M. Role of spinal microglia in rat models of peripheral nerve injury and inflammation. *Eur J Pain* 2007; **11**:223–230.
14 Molander C, Hongpaisan J, Svensson M, Aldskogius H. Glial cell reactions in the spinal cord after sensory nerve stimulation are associated with axonal injury. *Brain Res* 1997; **747**:122–129.
15 Nimmerjahn A, Kirchhoff F, Helmchen F. Resting microglial cells are highly dynamic surveillants of brain parenchyma in vivo. *Science* 2005; **308**: 1314–1318.
16 Wake H, Moorhouse AJ, Jinno S, Kohsaka S, Nabekura J. Resting microglia directly monitor the functional state of synapses in vivo and determine the fate of ischemic terminals. *J Neurosci* 2009; **29**:3974–3980.
17 Nakajima K, Tohyama Y, Maeda S, Kohsaka S, Kurihara T. Neuronal regulation by which microglia enhance the production of neurotrophic factors for GABAergic, catecholaminergic, and cholinergic neurons. *Neurochem Int* 2007; **50**:807–820.
18 Watkins LR, Milligan ED, Maier SF. Glial activation: a driving force for pathological pain. *Trends Neurosci* 2001; **24**:450–455.
19 Tsuda M, Shigemoto-Mogami Y, Koizumi S, Mizokoshi A, Kohsaka S, Salter MW, *et al.* P2X4 receptors induced in spinal microglia gate tactile allodynia after nerve injury. *Nature* 2003; **424**:778–783.
20 Jin SX, Zhuang ZY, Woolf CJ, Ji RR. p38 mitogen-activated protein kinase is activated after a spinal nerve ligation in spinal cord microglia and dorsal root ganglion neurons and contributes to the generation of neuropathic pain. *J Neurosci* 2003; **23**:4017–4022.
21 Tsuda M, Inoue K, Salter MW. Neuropathic pain and spinal microglia: a big problem from molecules in 'small' glia. *Trends Neurosci* 2005; **28**:101–107.
22 Smith JA, Das A, Butler JT, Ray SK, Banik NL. Estrogen or estrogen receptor agonist inhibits lipopolysaccharide induced microglial activation and death. *Neurochem Res* 2011; **36**:1587–1593.
23 Rupalla K, Allegrini PR, Sauer D, Wiessner C. Time course of microglia activation and apoptosis in various brain regions after permanent focal cerebral ischemia in mice. *Acta Neuropathol* 1998; **96**:172–178.

Original Article

Cephalalgia
An International Journal of Headache

International Headache Society

Cephalalgia
32(7) 518–527

DOI: 10.1177/0333102412444015
cep.sagepub.com

SAGE

Suppressive effect of chronic peroral topiramate on potassium-induced cortical spreading depression in rats

Miyuki Unekawa, Yutaka Tomita, Haruki Toriumi and Norihiro Suzuki

Abstract

Objective: To evaluate the chronic effect of topiramate (TPM) on cortical spreading depression (CSD), which is thought to be related to migraine aura.

Methods: Male rats (n = 30) were randomized to once-daily peroral treatment with TPM (50, 100, 200 or 600 mg/kg) or vehicle for 6 weeks. We evaluated the characteristics of CSD induced by topical application of KCl under isoflurane anesthesia and the changes in plasma level of TPM in each group. The effect of single administration of TPM on CSD was also evaluated.

Results: After the final administration of TPM, when the plasma level of TPM was high, KCl-induced CSD frequency and CSD propagation velocity were dose-dependently reduced and the interval between CSD episodes was elongated, compared with the vehicle control. However, before the final administration of TPM, when the plasma level was very low, the KCl-induced CSD profile was the same as that in the vehicle control. Single administration of TPM did not alter the CSD profile. Local cerebral blood flow was not significantly altered by chronic administration of TPM.

Conclusion: TPM suppressed the frequency and propagation of CSD along the cerebral cortex, and might be a candidate for relief of migraine.

Keywords

Topiramate, cortical spreading depression, chronic treatment, migraine, prophylaxis

Date received: 18 December 2011; revised: 2 February 2012; 22 February 2012; accepted: 9 March 2012

Introduction

Migraine is a common, chronic, incapacitating neurovascular disorder characterized by severe headache, autonomic nervous system dysfunction, and in some patients an aura involving neurologic symptoms (1). Recently developed selective serotonin receptor agonists, such as triptans, are useful to treat migraine, but strict compliance with the dosing schedule is essential for effective treatment. Furthermore, frequent migraine attacks may lead to excessive acute medication without proper supervision, potentially resulting in medication-overuse headache (2). Therefore, prophylaxis of migraine is an important goal.

The pathophysiology of migraine is very complex, but one of the main correlates is thought to be cortical spreading depression (CSD) (3,4). CSD is a transient neuronal depolarization that slowly propagates along the cerebral cortex, followed by long-lasting suppression of neuronal activity (5). It has been proposed that CSD is a neuronal mechanism underlying migraine aura (6) and is involved in vasodilation of the middle meningeal artery during headache, which is linked to changes of neurometabolic brain activity with transmission via the trigeminal nerve (7).

A β-adrenoceptor antagonist, propranolol, has been widely used in the prophylaxis of human migraine (8) and has been shown to suppress CSD in an animal model (9). However, the mechanism of its action remains unclear. Topiramate (TPM; 2,3:4,5-bis-*O*-(1-methylethylidene)-beta-D-fructopyranose sulfamate; $C_{12}H_{21}NO_8S$), which is used as an anticonvulsant

Keio University, Japan

Corresponding author:
Miyuki Unekawa, Department of Neurology, School of Medicine, Keio University, 35 Shinanomachi, Shinjuku-ku, Tokyo 160-8582, Japan
Email: unekawa.m@z5.keio.jp

monotherapy for epilepsy in many countries (10), is also a promising candidate for treatment of migraine. Several randomized, double-blind, placebo-controlled multicenter trials have demonstrated that TPM reduces the frequency of migraine and is well tolerated (11–14). It was also shown to improve workplace productivity and quality of life (15,16). The Prolonged Migraine Prevention with TPM (PROMPT) trial revealed that TPM reduced migraine auras in parallel with a reduction of headache, and the effects were similar in patients with and without aura (17). In addition, recent studies in experimental animals, as well as clinical observations, suggest that silent CSD may be involved in migraine without aura (18,19). Thus, there is interest in drugs that suppress CSD as candidates for preventive migraine treatment. The inhibitory effect of TPM on CSD has been investigated in experimental animals (20), including a chronic administration study in rats. In the present work, we examined in detail the effect of 6-week daily oral administration of TPM at various doses on potassium-evoked CSD in anesthetized rats.

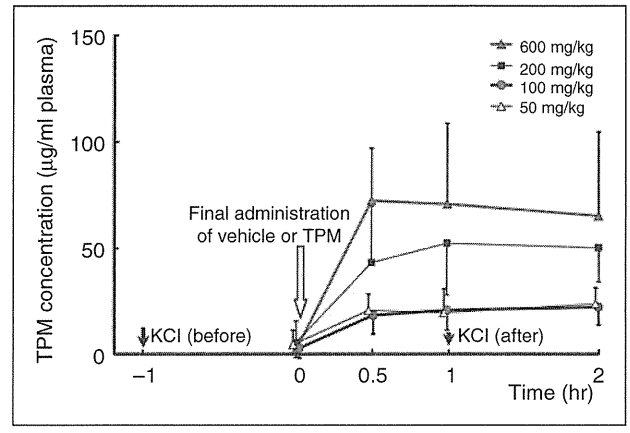

Figure 1. Plasma concentrations of TPM before and after the final administration of TPM on the day of CSD evaluation in chronically treated rats. An outlined arrow indicates the time of final intragastric administration of vehicle/TPM ($t = 0$) and solid arrows indicate the times of KCl application on the surface of the brain [KCl (before) at $t = -1$ and KCl (after) at $t = 1$].

Materials and methods

General procedures of chronic study

Animals were used with the approval (No. 09058) of the Animal Ethics Committee of Keio University (Tokyo, Japan), and all experimental procedures were in accordance with the university's guidelines for the care and use of laboratory animals. Male Sprague-Dawley rats (8–9 weeks, initial body weight; 412 ± 28 g, $n = 30$) were randomized to five groups so that the mean body weights were not significantly different among groups: a vehicle group (0.5% methylcellulose: 400 cps (centipoises); Sigma Aldrich Japan, Tokyo, Japan) and four TPM groups (50 mg/kg, 100 mg/kg, 200 mg/kg, 600 mg/kg; provided by Janssen Pharmaceutical K.K., Tokyo, Japan). Test solution was adjusted to 5 ml/kg and administered by gavage once daily for 6 weeks. During the administration period, rats received food and water ad libitum. The animals were kept in an air-conditioned room maintained at 23.0 ± 1.0°C and 55 ± 7% humidity with automatic lighting between 08:00 and 20:00. Body weight was monitored daily throughout the treatment period.

Procedures of CSD measurement

On the final treatment day, the animals were anesthetized with isoflurane (2.5–3.0%) and subjected to CSD evaluation as previously reported (21). Briefly, each rat was fixed to a head-holder (SG-3 N modified to be flexible around the horizontal axis, Narishige Scientific Instrument Lab., Tokyo, Japan) and a cranial window of approximately 4 mm in diameter was opened in the left side of the skull at the parieto-temporal region of the cerebral cortex. The dura was removed and the exposed cortex was covered with a cover slip to prevent it from drying out. CSD was induced by introducing a drop (5 μl) of 1.0 M KCl solution into an additional posterior hole of 2 mm in diameter, centered at the coordinates of 7 mm posterior and 2 mm lateral to the bregma. Approximately 1 h after the first KCl application, when no further CSD had occurred for more than 10 min, vehicle or TPM was administered through an intragastric catheter. The second application of KCl was performed 1 h after the final administration of vehicle or TPM, as shown in Figure 1. Arterial blood pressure (ABP) was continuously recorded through a femoral arterial catheter via a surgical strain gage (MLT0670 and ML117, ADInstruments Pty. Ltd., Bella Vista, NSW, Australia). Heart rate (HR) was determined from the ABP wave. Continuous recordings of ABP, HR, cerebral blood flow (CBF) and direct current (DC) potential (see below) were acquired with a multi-channel recorder (PowerLab 8/30, ADInstruments Pty. Ltd.) and recorded with proprietary software (LabChart, ADInstruments Pty. Ltd.) for offline analysis. All procedures were performed at constant body temperature, maintained with a heating-pad and thermocontroller (BWT-100, Bioresearch Center Co., Ltd., Nagoya, Japan). CSD was elicited with KCl solution after confirmation that all parameters had remained stable for at least 10 min.

Table 1. Physiological parameters just before CSD evaluation in chronically treated rats

		Before the last administration		After intragastric administration	
Treatment group	Body weight (g)	MABP (mmHg)	HR (bpm)	MABP (mmHg)	HR (bpm)
Vehicle	545 ± 34	74 ± 10	313 ± 57	83 ± 18	341 ± 50
Topiramate 50 mg/kg	536 ± 41	85 ± 12	349 ± 49	86 ± 10	321 ± 28
Topiramate 100 mg/kg	514 ± 53	75 ± 4	295 ± 17	83 ± 10	285 ± 21
Topiramate 200 mg/kg	509 ± 25	74 ± 10	295 ± 18	76 ± 17	282 ± 25
Topiramate 600 mg/kg	482 ± 24[a]	84 ± 7	317 ± 36	86 ± 10	300 ± 42

HR, heart rate; MABP, mean arterial blood pressure.
[a]$p<0.05$ significant difference from the vehicle control.

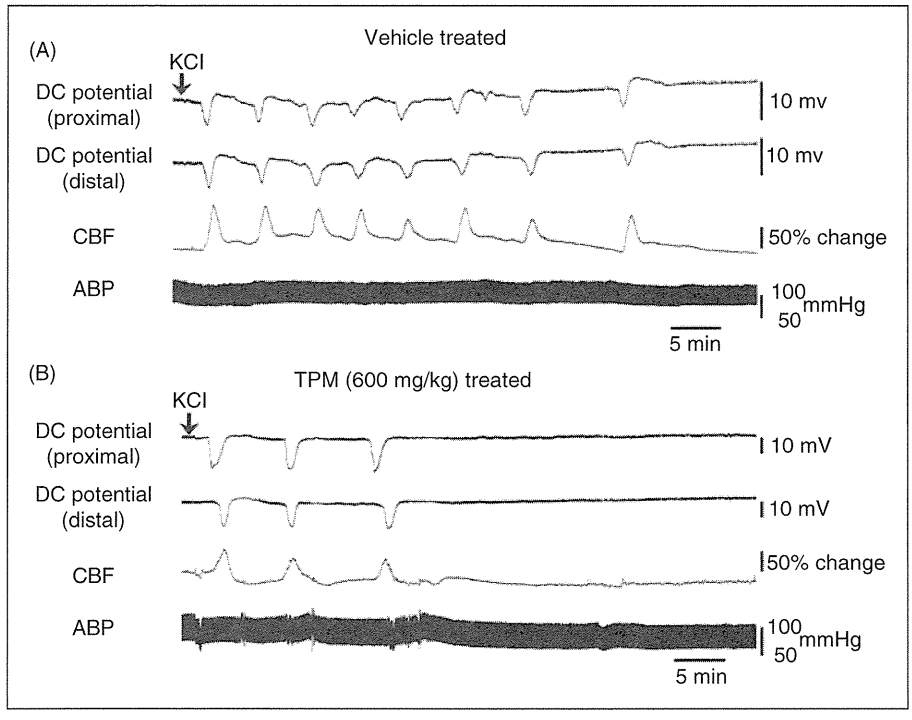

Figure 2. Original recordings of DC potential at the proximal and distal sites, as well as CBF and ABP. KCl was applied on the brain surface at the arrows, 1 h after the final administration of vehicle (A) or 600 mg/kg of TPM (B) in rats treated for 6 weeks.

Measurements of DC potential and CBF

Two Ag/AgCl electrodes (tip diameter = 200 μm, EEG-5002Ag, Bioresearch Center Co., Ltd.) were inserted 200 μm under the pia mater at the anterior edge (0.5 mm posterior and 2 mm lateral to bregma) and posterior edge (3.5 mm posterior and 2 mm lateral to the bregma) of the cranial window, and immobilized with dental cement. Ag/AgCl reference electrodes (EER-5004Ag, Bioresearch Center Co., Ltd.) were subcutaneously placed in the space between the skull-bone and the scalp. DC potential was amplified at 1–100 Hz and digitized at 1 kHz with a differential headstage and differential extracellular amplifier (Model 4002 and EX1, Dagan Co., Minneapolis, MN, USA).

CBF was monitored with a laser Doppler flowmeter (LDF) (ALF 21 R, Advance Co., Ltd., Tokyo, Japan). The probe, which had a diameter of 0.8 mm, was placed on the surface of the cortex 2 mm posterior and 2 mm lateral to the bregma (intermediate region of the cranial window).

Evaluation of CSD susceptibility

One application of KCl induced repetitive negative deflections of DC potential (i.e., CSD). CSD was detected at the posterior site (proximal) and then at the anterior site (distal) after a delay. At the same time, CBF was elevated, as reported previously (21). We defined CSD as the occurrence of DC potential

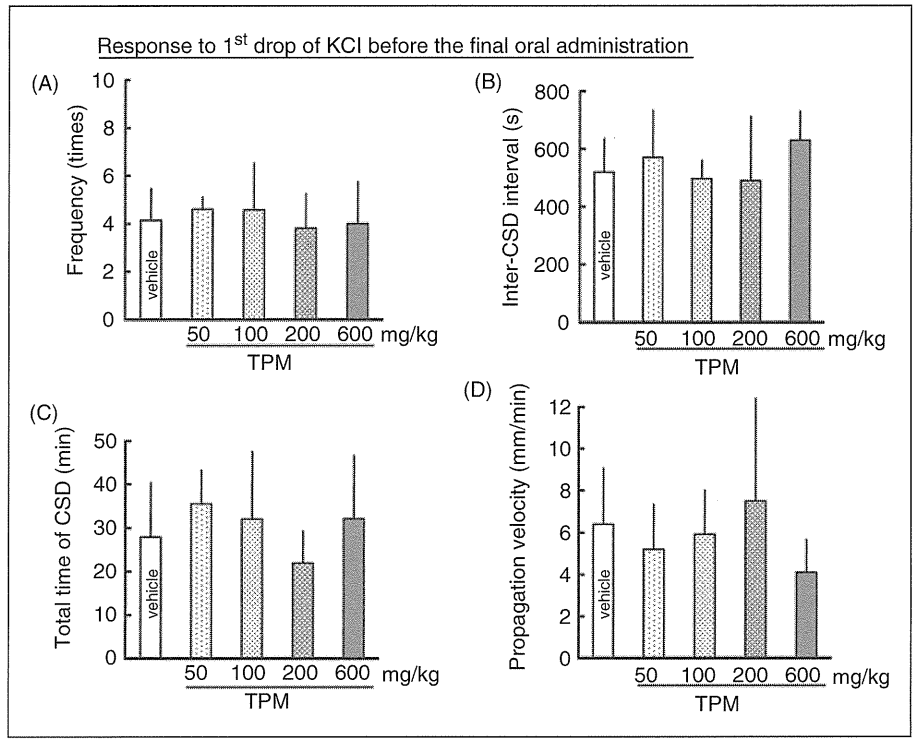

Figure 3. Average values of CSD occurrence frequency (A), inter-CSD interval (B), total length of time for which CSD continued (C) and CSD propagation velocity (D) in response to KCl application 1 h before the final oral administration of vehicle/TPM in chronically treated rats (t = −1 in Figure 1). The results in TPM-treated groups are not statistically significantly different from the vehicle control.

deflections detected at both sites, together with CBF elevation. We evaluated CSD occurrence frequency, interval between CSD episodes, and total length of time for which CSD continued (duration from the first CSD to the last CSD). Propagation velocity from the proximal to the distal site was also calculated based on the distance between the electrodes.

Measurement of plasma level of TPM

Before the final administration of TPM (time 0), and at 30 min, 60 min, and 120 min after the final intragastric administration of TPM, as shown in Figure 1, arterial blood was collected through the arterial catheter. After protein precipitation with acetonitrile, plasma samples were used for measurement of the plasma level of TPM by means of a validated liquid chromatography–tandem mass spectrometry (LC-MS/MS) method (22) with some modifications. Separation was done on a reversed-phase LC column (X-Bridge C18 3.5 μm – 50 × 4.6 mm, Waters, Milford, USA) with a mixture of 10 mM ammonium acetate and acetonitrile as the mobile phase. Detection was by tandem MS on an API-3000 MS/MS (Applied Biosystems, Toronto, Canada), operated in the negative ion mode using the TurboIonSpray™-interface. TPM was monitored at the *m/z* transition 338.1 → 78.0 using a dwell time of 300 ms. The limit of quantification was 50 ng/ml. In measurement of independent QC samples, the intra-batch accuracy was between 85% and 115%.

Acute effect of TPM on CSD

Male Sprague-Dawley rats (12–19 weeks, body weight; 519 ± 95 g, n = 7) were used for evaluation of the effect of single administration of TPM. Using the same protocol as described for chronically treated rats, we evaluated the KCl-induced CSD profile and CBF before and after intragastric administration of TPM (600 mg/kg). Changes of ABP, HR and blood gas level were followed. Arterial blood gas analysis was performed with a RapidLab 348 (Siemens AG, Munich, Germany).

Statistical analysis

All data are reported as means ± SD. Multiple comparisons were performed using Dunnett's test among vehicle and TPM chronic administration groups. The paired t-test was used to evaluate the acute effect of TPM on the CSD profile versus the pre-administration

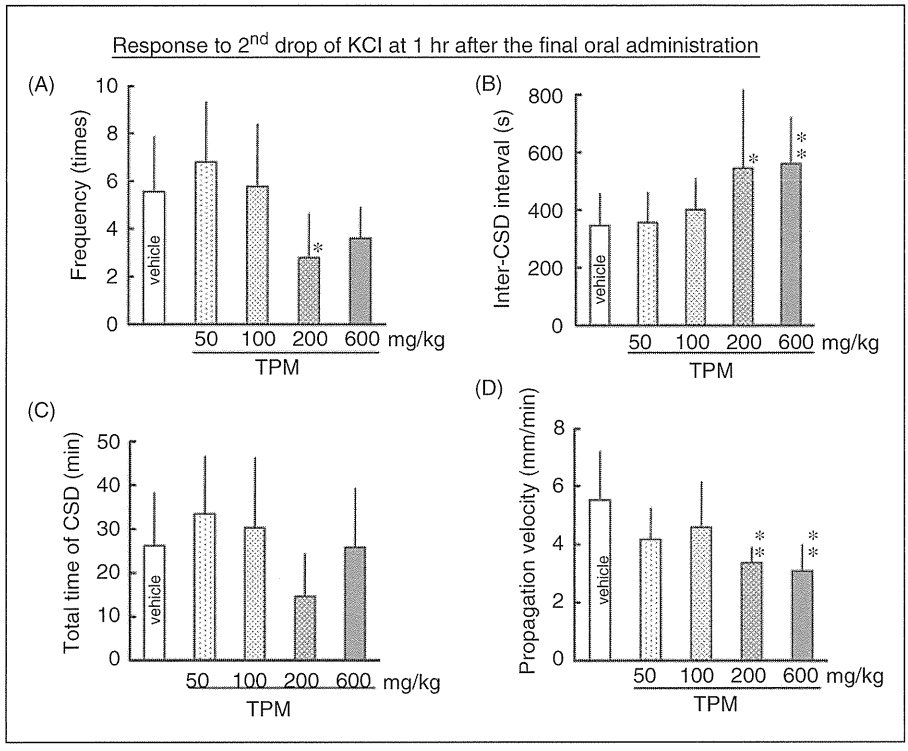

Figure 4. Average values of CSD occurrence frequency (A), inter-CSD interval (B), total length of time for which CSD continued (C) and CSD propagation velocity (D) in response to KCl application 1 h after the final oral administration of vehicle/TPM in chronically treated rats (t = 1 in Figure 1). *p < 0.05, **p < 0.01 significant differences of the TPM-treated groups from the vehicle control.

level. A p value of <0.05 versus the vehicle treatment group or the pre-administration level was considered to be statistically significant.

Results

Plasma level of TPM

The plasma level of TPM increased rapidly after administration, and a dose-dependent plateau level was maintained for 2 h (Figure 1). After 6 weeks of daily administration, the plasma level of TPM before the final administration was 1/5 to 1/50 of the maximum level; that is, there was no indication of TPM accumulation. After intraperitoneal administration of 200 or 500 mg/kg TPM, the plasma level reached a maximum of 125 ± 14 or 155 ± 98 μg/ml, respectively, within 1 h after administration. The maximum plasma level after intragastric administration was approximately 1/3 of that after intraperitoneal administration and remained at a plateau level for a longer period.

Effect of chronic TPM on CSD

Physiological parameters just before CSD evaluation in each group are shown in Table 1. Although dose-dependent suppression of growth was observed, physiological parameters were not significantly different among the treated group. Neither mortality nor abnormal behavior was observed in any animal during the treatment period. Therefore, we concluded that the physiological state of the animals was not impaired.

As shown in Figure 2A, one application of KCl induced repetitive (between 2 and 8 times) negative deflections of DC potential (i.e., CSD). CSD was detected first at the posterior (proximal) site, and then at the anterior (distal) site with a delay time of 14 to 80 s. After the final administration of TPM, CSD occurrence was slightly suppressed (Figure 2B). No CSD-associated change of ABP was seen in any rat. Mean arterial blood pressure (MABP) was maintained within ± 20 mmHg in each rat throughout the experiments, and did not decrease below 60 mmHg in any rat.

In the observation 1 h before the final oral administration of TPM, none of CSD occurrence frequency, inter-CSD interval, total length of time for which CSD continued or propagation velocity was statistically significantly different from the value in the vehicle group (Figure 3). However, 1 h after the final oral administration of TPM, during the plasma TPM level plateau period, CSD occurrence frequency was dose-dependently decreased, inter-CSD interval was

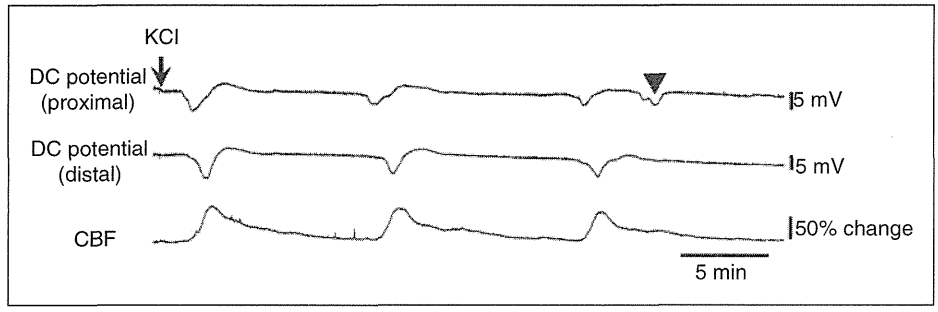

Figure 5. Original recordings of DC potential at the proximal and distal sites and CBF showing an example of non-propagated DC potential deflection. DC potential deflection detected at the proximal site was not propagated to the distal site, as indicated with an arrowhead, and there was no CBF change.

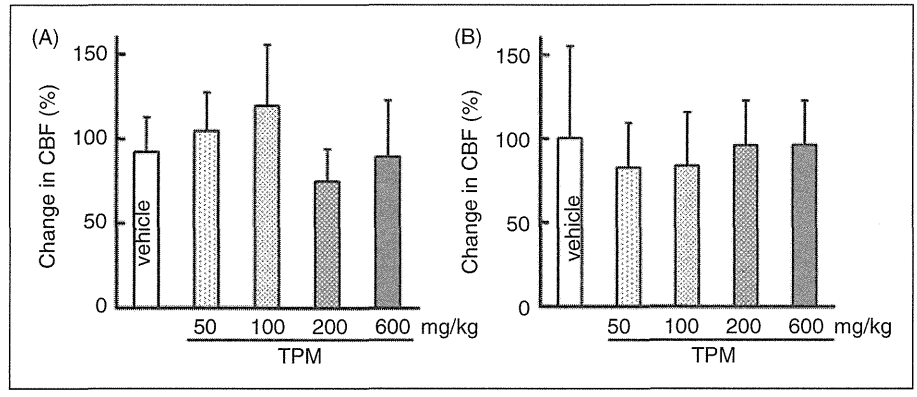

Figure 6. Average values of CSD-associated CBF changes in response to KCl application before the final oral administration of drugs ($t = -1$ in Figure 1) (A) and those in response to KCl application after the final oral administration of drugs ($t = 1$ in Figure 1) (B). There are no statistically significant differences from the vehicle control.

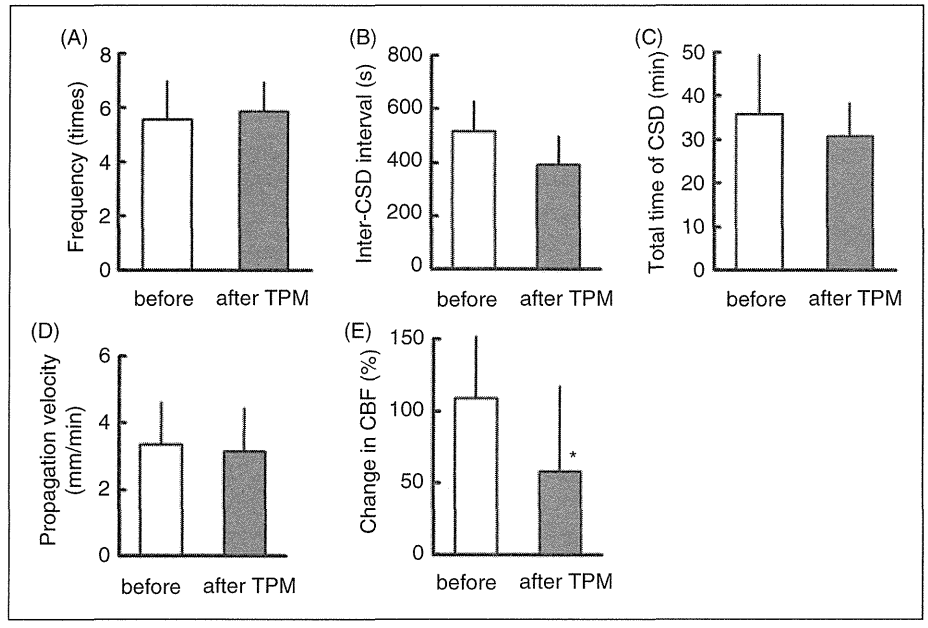

Figure 7. Changes of CSD occurrence frequency (A), inter-CSD interval (B), total length of time for which CSD continued (C), CSD propagation velocity (D) and CSD-associated CBF changes (E) from the pre-administration level (before) to the level after single gavage administration of TPM (600 mg/kg). *$p < 0.05$ significant difference from the pre-administration level.

Table 2. Changes in physiological parameters, arterial pH and arterial blood gas in response to CSD induction with KCl application

	MABP (mmHg)	HR (bpm)	pH	PaO_2 (mmHg)	$PaCO_2$ (mmHg)
Before administration of topiramate					
Before KCl	80 ± 5	320 ± 22	7.46 ± 0.01	84 ± 8	39 ± 3
After 1 h	80 ± 6	308 ± 24	7.45 ± 0.03	78 ± 10	38 ± 3
After intragastric administration of topiramate					
Before KCl	82 ± 14	298 ± 36	7.42 ± 0.04	88 ± 9	38 ± 4
After 1 h	76 ± 13	288 ± 32	7.41 ± 0.04	81 ± 6	40 ± 4

HR, heart rate; MABP, mean arterial blood pressure; PaO_2, partial pressure of arterial oxygen; $PaCO_2$, partial pressure of arterial carbon dioxide.

elongated, and propagation velocity was decreased. The total length of time for which CSD continued showed a tendency to decrease, but this was not significant (Figure 4). A small negative deflection of DC potential only at the proximal site but not at the distal site, with a small CBF change or with no CBF change, was detected in seven rats (three rats in the 600 mg/kg group, two rats in the 100 mg/kg group, one rat in the 50 mg/kg group and one rat in the vehicle group) (Figure 5). There was no difference in the CSD-associated elevation of CBF before and after the final administration of TPM (Figure 6).

Acute effect of TPM on CSD

KCl-induced CSD susceptibility (CSD occurrence frequency, inter-CSD interval, propagation velocity and total length of time for which CSD continued) was not significantly influenced, but CSD-associated elevation of CBF was significantly reduced by single administration of TPM (Figure 7). Negative deflection of DC potential only at the proximal site but not at the distal site, with or without a small CBF change, was detected in five rats after TPM administration. Physiological parameters (MABP, HR, arterial pH, partial pressure of arterial oxygen (PaO_2) and carbon dioxide ($PaCO_2$)) were within normal ranges and were not significantly changed either by KCl application or by intragastric administration of TPM (Table 2).

Discussion

In our study, chronic peroral administration of TPM suppressed CSD susceptibility, whereas single administration had little effect on CSD susceptibility. Intraperitoneal administration of TPM for 4 weeks suppressed CSD occurrence frequency induced by KCl application, enhanced the cathodal stimulation threshold and lowered the propagation speed, and longer administration (17 weeks) almost abolished CSD occurrence (23). Thus, oral administration for a longer period would be expected to have a potent effect on CSD susceptibility.

The administered amount and plasma concentration of TPM in the present experiment were much higher than the clinically used levels in human. We demonstrated rapid and stable absorption of orally administered TPM in this study. However, the TPM concentration before the final administration was very low in this experiment, indicating that TPM was largely eliminated within 1 day in rats, and no accumulation effect was observed during daily administration for 6 weeks. The biological half-life ($T_{1/2}$) in humans is 27–31 h (24). Thus, species difference in TPM turnover rate and/or bioavailability might require a higher dose in rats, and drug accumulation might also be different. We found that CSD occurrence and propagation before the final dose of TPM in the 6-week daily administration protocol were not different from those of the vehicle control. This suggests that there might be a drug threshold of approximately 25 μg/ml in rats. This in turn might be consistent with the observation in the PROMPT trial that cessation of chronic TPM resulted in loss of the prophylactic effect (25), and suggests that monitoring of plasma TPM levels might be important for effective treatment.

Single gavage administration of TPM had no effect on CSD susceptibility in our experiment. It was also reported by others that single intraperitoneal administration did not reduce the number of CSD episodes induced by KCl (23). These facts may suggest that a certain period is required for manifestation of the prophylactic effect of TPM. However, a single dose of intravenous TPM inhibited CSD occurrence induced by needle plunge, but did not influence the CSD propagation speed in anesthetized rats and cats (20). One possible explanation might be a time lag in the transfer of TPM from blood to brain. It is also possible that there is a depot effect due to drug accumulation within a sequestered brain compartment. Although it is possible that a single dose might block propagation in the distal direction as seen in our experiment, a similar phenomenon was also seen in chronically treated rats. CSD seems to be more effectively suppressed by chronic treatment. Although intravenous injection might provide rapid relief of migraine, it may be possible to